ESCUELA TÉCNICA SUPERIOR DE INGENIEROS INDUSTRIALES Y DE TELECOMUNICACIÓN

Titulación :

INGENIERO INDUSTRIAL

Título del proyecto:

MULTI SOURCE POWER PATH MANAGEMENT FOR COMPLEMENTARY BALANCED EMBEDDED ENERGY HARVESTING APPLICATIONS

Maite Muruzabal Fernández

Tutor: Pablo Sanchis Gúrpide

Pamplona, 28 de junio de 2014

Vrije Universiteit Brussel

upna Universidad Pública de Navarra
Nafarroako Unibertsitate Publikoa

Multi Source Power Path Management for Complementary Balanced Embedded Energy Harvesting Applications

Author: Maite MURUZABAL FERNANDEZ

Supervisors: Prof. Yannick VERBELEN
Prof. Dr. Abdellah TOUHAFI

Thesis Submitted in Partial Fulfillment of the Requirements of the Degree of Master in Engineering Technology

Academic Year 2013 - 2014

Multi Source Power Path Management for Complementary Balanced Embedded Energy Harvesting Applications

Maite Muruzabal Fernandez

2013 - 2014

Abstract

The main focus of this Thesis was to design a complementary balanced energy harvesting system to increase the reliability of embedded electronic applications by extracting power from multiple sources.

Microchip XLP 16-bit Energy Harvesting Development Kit was tested and several solar, piezoelectric, and thermoelectric energy harvesters commercially available were reviewed and parameterized, calculating their efficiencies compared to the ideal performance.

Finally, a power path was designed and implemented in a multi-source energy harvesting system, enabling it to simultaneously scavenge energy from light, vibrations and temperature differences.

The results obtained did not support the expectations, due to a mismatch between the transducers used and the load. However, it can be concluded that the work done can still be a good starting point for future research on this subject.

Multi Source Power Path Management for Complementary Balanced Embedded Energy Harvesting Applications

Maite Muruzabal Fernandez

2013 - 2014

Resumen

Esta tesis tenía como objetivo principal el desarrollo de un sistema de recolección equilibrada de energía, para aumentar la fiabilidad de aplicaciones electrónicas embebidas mediante la extracción de energía de múltiples fuentes.

Durante el desarrollo de la tesis se utilizó el *XLP 16-bit Energy Harvesting Development Kit* de Microchip, y se probaron diferentes transductores solares, piezoeléctricos y termoeléctricos disponibles comercialmente, realizando su parametrización y calculando su eficiencia en condiciones no ideales.

Por último, se diseñó e implementó un circuito para la gestión de la potencia en un sistema de recolección de energía, de modo que se extrajera energía procedente de luz, vibraciones y gradientes térmicos de forma simultánea.

Aunque no se obtuvieron los resultados esperados, debido a una discordancia entre la carga y los transductores, se puede concluir que el trabajo realizado constituye un buen punto de partida para investigaciones futuras.

Acknowledgements

First of all, I would like to express my sincere gratitude to my main supervisor, Professor Yannick Verbelen, for giving me the opportunity to research on this interesting field, and being supportive and patient through all the process.

I would also like to thank Professor Jelmer Tiete and Professor Doctor Kris Steenhaut, who helped me in the first phase of my thesis and helped me find a subject that really interested me. If it had not been for them, I would have never met my supervisor and would have not been able to find this fascinating subject.

I wish to thank Professor Doctor Pablo Sanchis Gúrpide, my supervisor in Spain, and all the colleagues from the Rapptor laboratory, as well as the staff of the university who have helped me during these months.

Furthermore, I would also like to acknowledge the opportunity provided by the Public University of Navarre and the Erasmus Programme, which made it possible to do my Master's Thesis at the Vrije Universiteit Brussel.

Finally, special thanks to my family and friends, who have encouraged me during the whole degree, and especially, during the preparation of this thesis.

Contents

1 Introduction **1**

2 Energy harvesting: State-of-the-art **2**
2.1 Harvesting energy from vibrations 2
2.2 Harvesting energy from light 4
2.3 Harvesting energy from thermal sources 6
2.4 Multi-source Energy Harvesting 7

3 Energy Harvesting System Design **9**
3.1 Energy harvesting Development Kit 10
3.2 Piezoelectric Transducer 11
3.3 Thermoelectric Transducer 13

4 Starting with the XLP 16-bit Energy Harvesting Development Kit **15**

5 Parametrization of generator efficiency **17**
5.1 Photovoltaic Panel 17
5.1.1 First panel 18
5.1.2 Second panel 20
5.2 Thermoelectric transducer 25
5.2.1 Nextreme eTEG HV37 25
5.2.2 Micropelt TGP-651 27
5.2.3 Marlow EHA-PA1AN1-R02-L1 29
5.3 Piezoelectric transducer 31
5.4 Summary and conclusions 36

6 Power Path Management **38**
6.1 Power Path Design 38
6.1.1 Solar Energy Harvesting System 39
6.1.2 Piezoelectric Energy Harvesting System 40
6.1.3 Thermoelectric Energy Harvesting System 40
6.1.4 Battery charger circuit 42
6.1.5 Microcontroller 43
6.2 Implementation and Results 48

7 Conclusions and Future Work **54**

Bibliography **55**

List of Figures

2.1 Vibration energy harvester model 4
2.2 Photovoltaic cell model 5
2.3 Load lines of a solar cell 5
2.4 Photovoltaic cell power curve 6
2.5 Schematic of a thermocouple 7
2.6 Schematic of a thermopile 7

3.1 EnerChip EVAL-08 Demo Kit Block Diagram 11
3.2 Microchip's XLP 16-bit Energy Harvesting Development Kit 11
3.3 V21BL piezoelectric harvester 12
3.4 V22B piezoelectric harvester 12
3.5 V22BL piezoelectric harvester 12
3.6 Nextreme eTEG HV37 13
3.7 Micropelt TGP-651 14
3.8 Marlow's Thermal EH Demo Unit 14

4.1 Realterm screenshot: demonstration application 15

5.1 Testing device designed by Davy Van Belle 18
5.2 First photovoltaic cell 19
5.3 Output power and current for incandescent lamp (First cell) 19
5.4 Output power and current for halogen lamp (First cell) 20
5.5 Second photovoltaic cell 20
5.6 Output power and current for incandescent until 1000 lux (Second cell) . . 21
5.7 Output power and current for halogen lamp until 1000 lux (Second cell) . . 21
5.8 Output power and current for LED lamp until 1000 lux (Second cell) 22
5.9 Output power and current for fluorescent lamp until 1000 lux (Second cell) 22
5.10 U-I and power curves at 1000 lux for incandescent lamp (Second cell) . . . 23
5.11 U-I and power curves at 1000 lux for halogen lamp (Second cell) 23
5.12 U-I and power curves at 1000 lux for LED lamp (Second cell) 24
5.13 U-I and power curves at 1000 lux for fluorescent lamp (Second cell) 24
5.14 U-I curves at 200 lux for all lamps (Second cell) 25
5.15 The system used to achieve temperature differences 26
5.16 Output current and power against estimated thermal gradients 27
5.17 Setup to measure the temperature difference 28
5.18 Open-circuit voltage and power for different thermal gradients 28
5.19 Marlow's unit with the wire harness and the power resistor used 29
5.20 Maximum output power in function of the temperature difference 30
5.21 Output current and power for different loads 31
5.22 Output power against thermal gradient for a constant load 31

5.23 Using a speaker as a shaker 32
5.24 Structure built to fix the piezoelectric harvesters 33
5.25 V21BL open-circuit voltage at 50 Hz (4.8 grams) 33
5.26 V21BL open-circuit voltage at 55 Hz (4.8 grams) 33
5.27 Setup including an accelerometer to measure the amplitude of the vibration 34
5.28 Output power from V21BL harvester for different loads 35
5.29 Output power from V22BL harvester for different loads 35
5.30 Output power from V22B harvester for different loads 36

6.1 Schematic diagram of the circuit designed 39
6.2 Solar energy harvesting circuit 40
6.3 Piezoelectric energy harvesting circuit 40
6.4 Logic circuit implemented to select the output voltage 41
6.5 Thermoelectric energy harvesting circuit 42
6.6 Battery charger circuit 43
6.7 Schematic switch circuit 44
6.8 Sequence of commutation when all the MOSFETs must be switched on . . 44
6.9 Procedure followed by the microcontroller to control the transistors 46
6.10 Schematic of the whole circuit, excluding the logic circuit and the microcontroller 47
6.11 PIC24F16KA102 Pin diagram 48
6.12 Prototype implementation 49
6.13 Thermoelectric circuit implementation 50
6.14 Implementation of the rest of the circuit 50
6.15 Configuration using p-MOSFETS 51
6.16 Information in the terminal program 52
6.17 Gate Voltage of solar and thermoelectric MOSFETs 53
6.18 LED connected to the LTC4071 as a load 53

List of Tables

3.1 Comparison between two energy harvesting development kits 10
3.2 Characteristics of Mide Volture piezoelectric transducers 13

5.1 Output power and efficiency at 1000 lux for different lamps 25
5.2 Piezoelectric Harvesters' Natural frequencies for different tip masses 34
5.3 Maximum output power for different energy sources and harvesters 37

6.1 LTC3109 Output voltage configuration 41
6.2 Nomenclature used in Figure 6.9 45
6.3 Microcontroller pins assignment 48

Chapter 1

Introduction

Energy harvesting or energy scavenging is the process by which the energy available in the environment (light, wind, mechanical movement, thermal gradients, etc) is stored or is used to power a load.

In the recent years, energy harvesting has become very important due to the development of low power systems, such as wearable electronic devices (biomedical implants, watches, etc) or wireless sensor networks [1, 2].

In a sensor network, many sensor nodes are spread over an area and communicate among themselves by radio waves. These sensor nodes need power to take measurements and make the communications, but powering them with batteries is highly inefficient and expensive, as those batteries may need to be replaced by the end of their useful life, which is usually a few years for the most commonly used primary batteries [3, 4]. Sometimes this is not even an option, like when the nodes are located in remote or unreachable places. For example, in environmental monitoring in wilderness areas like a volcano, or in structural health monitoring in a bridge, where hundreds of sensors are needed [5, 6].

Moreover, the use of electronic devices has become generalised in our society, with increasingly powerful applications. However, these devices still need a battery, which can be rechargeable or not. For example, in the case of pacemakers the battery must be changed every 6-10 years, requiring surgery [7]. In the situations mentioned before, energy harvesting becomes a great alternative, as the environmental energy can be used to extend the battery lifetime or even to replace it.

Considerable research has been done on energy harvesting, especially on solar energy. However, most of the studies are focused on harvesting energy from one unique source. The aim of this thesis is to develop a complementary balanced energy harvesting system, which can harvest energy from three different sources and combine them efficiently to power a load. Although it is focused on low power applications, its results could be scaled for any application where there is environmental energy available [4].

Chapter 2

Energy harvesting: State-of-the-art

With the recent development of wireless sensor networks and electronic portable devices, it has become evident that energy supply is the most limiting factor. Although battery technology is continuously improving, when long lifetime is needed, their use often results in bigger devices or in higher maintenance costs [2, 8]. This fact becomes particularly important in wireless sensor applications, where many sensor nodes can be located in remote areas where replacing the batteries may be unfeasible. Moreover, batteries must be manually replaced by a technician, leading to higher costs.

Energy harvesting becomes a great solution, as obtaining energy from the environment results in extended battery lifetime or it can even eliminate the need of an energy storage device in some low-power applications. A wide variety of applications can benefit from energy scavenging: biomedical implants, automotive, watches, predictive maintenance of structures and machines, weather stations, etc [1, 6].

There are multiple energy harvesting sources [1]. Some of them are:

- Solar and indoor light. Although the energy available indoors is much lower than outdoors, it is still a good option for low-power applications.
- Temperature differences. For example, we can find thermal gradients between the environment and a machine hull or the surface of a hot or cold pipe.
- Pressure gradients
- Motion or vibration present in floors, stairs, engines, door frames, human body, etc.
- Electromagnetic (RF): radio, TV, wireless internet, etc.
- Mechanical energy: water flowing in a pipe, wind flow, etc

In the following sections we will develop the state-of-the-art of light, vibrations and thermal energy sources, as these are the sources that will be used in our energy harvesting system.

2.1 Harvesting energy from vibrations

As we have said, there are multiple sources of mechanical motion in the environment: industrial machines, bridges, windows next to a busy road, floors, door frames, stairs,

human body movement, etc [9, 10]. This energy can be harvested with an appropriate mechanical-to-electrical generator. Most of the vibration energy harvesters available can be modelled by a resonant mass-spring system (Figure 2.1), where the kinetic energy of the mass is converted into electrical energy [10]. Up to date, there are three kinds of vibration energy harvesters [2, 8, 9, 11]:

- Electrostatic mechanisms
  These generators use vibrations to vary the distance between the two plates of a charged capacitor against the electrostatic force, increasing the energy stored in the capacitor.

  The principal advantage of electrostatic transducers is the ease of integration in microsystems, but their main disadvantages are that they need an input voltage to start operating, and their output voltage and impedance are too high, resulting in reduced current supply.

- Electromagnetic mechanisms
  These transducers are based on Faraday's law of electromagnetic induction. In these devices, the relative movement of a magnetic core with respect to a coil causes a variation in the magnetic flux, generating an AC voltage across the coil and a current in the electrical load.

  These devices require no input voltage source, but the voltage generated is usually below 0.5 V [8, 9]. Moreover, it is difficult to have a small-size efficient transducer. The most common application of this technology has been, during many years, a bicycle dinamo, but it is believed that its applications will increase in the next years. In fact, the japanese company Brother Inc. has already designed a prototype of a electromagnetic transducer shaped like an AA battery, that could be used, for example, in remote controls [12].

- Piezoelectric mechanisms
  They are based on the piezoelectric effect, using vibrations to produce a mechanical stress in a piezoelectric material so that a voltage is generated.

  These devices do not require an input voltage and can be used in either macro- or microscaled applications. Moreover, their output voltage is higher than that of electromagnetic devices (between 3 and 8 V [9]), so they usually do not require transformers. These characteristics make them a suitable solution for various applications, such as portable electronic devices [13] or pacemakers [7], although their use is still in an experimental phase. In our system, we will use a piezoelectric harvester because of their simplicity and better performance compared with the other two types.

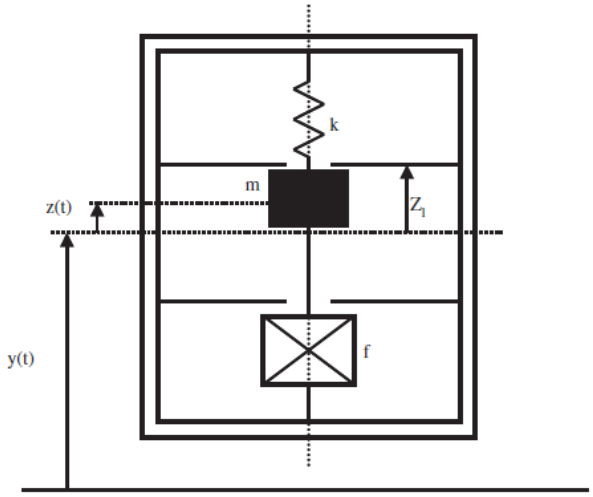

Figure 2.1: Vibration energy harvester model [14]

Piezoelectric harvesters produce AC power, so their output needs to be rectified before connecting it to the load. Several manufacturers, like Mide or Linear Technology, offer integrated circuits that include a bridge rectifier. Mide offers either the EHE001 board, which provides an unregulated DC output, or the EHE004, with a regulated output, and both can be easily connected to the Volture harvesters. Linear Technology proposes the LTC3588-1, which is a chip designed for piezoelectric energy harvesting applications, and it includes a full-wave bridge rectifier and a buck converter [15]. For our system, we choose the solution offered by Linear Technology because it seems more flexible for our application and, in addition, we can order free samples from their webpage.

2.2 Harvesting energy from light

Solar and indoor light have been used as an energy source for decades. Solar cells are based on the photovoltaic effect to convert the incident light into electrical energy. They present many advantages, like their modularity or lack of emissions, but they have low efficiencies and intermittent operation, as they depend on the light availability [8].

Comercial solar cells' efficiencies depend on the material used, but they are usually between 5% and 30%, and they can produce until $1\,\mathrm{mWcm^{-2}}$ under indoor illumination [8, 10, 11]. Most of the PV-cells comercialised are made of silicon, but great effort is being made to produce efficient and cheaper cells made of different materials, such as CdTe, GaAs, CIS (Copper Indium Selenide), perovskite or organic materials [16–19].

Photovoltaic cells can be modelled as a DC current source with a diode in parallel, as shown in Figure 2.2, and they are characterized by their open-circuit voltage and their short-circuit current [20]. The current produced by the cell is proportional to its area, its efficiency and the irradiance. The voltage is a function of the current through the cell and it is usually low, so it must be increased with a DC/DC converter to the level required by the load.

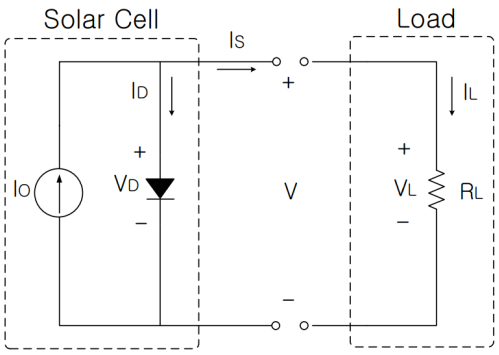

Figure 2.2: Photovoltaic cell model [21]

In this model, I_O is proportional to the light intensity, and if it increases, it will flow to the load until the voltage V_L is 0.7 V, when the diode turns on. Then, the voltage in the load will be 0.7 V, and the current will be $I_L = 0.7/R_L$. Figure 2.3 represents some load lines of a solar cell, where the shaded area represents the harvested power transferred to the load. The output power will depend on the slope of the load line, which is inversely proportional to the load.

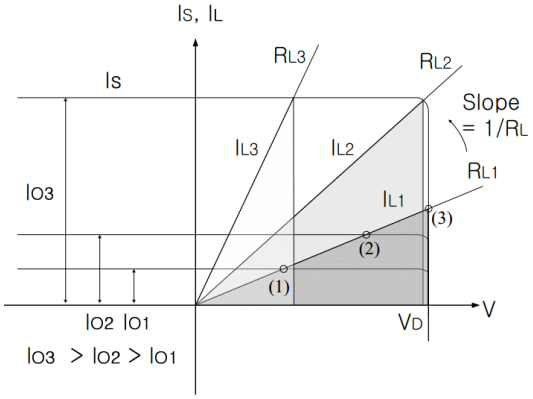

Figure 2.3: Load lines of a solar cell [21]

The optimal value of voltage and current for power extraction is called the maximum power point (MPP). As we have said, it depends on the light intensity, so to maximize the efficiency it is necessary to track this point continuously. The power curve for a PV cell shows that the corresponding voltage to this point is 75-80% the open-circuit voltage, and if the operation voltage is higher than this one, the power generated will decrease considerably, given that the curve slope is much steeper in this part [20], as can be observed in Figure 2.4.

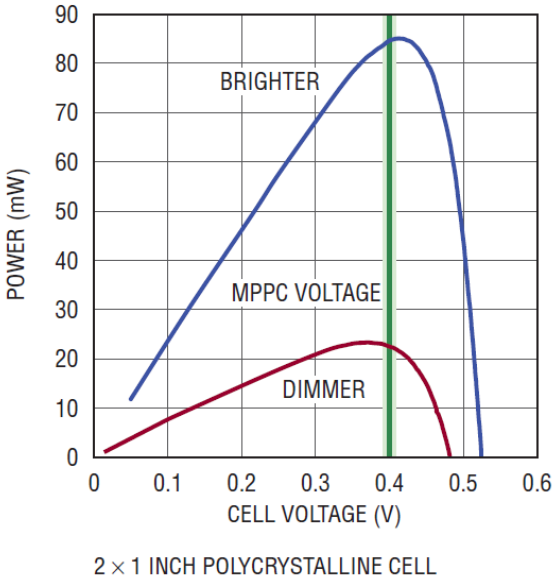

Figure 2.4: Photovoltaic cell power curve [20]

As we have mentioned before, photovoltaic cells produce low DC voltage, although several cells can be connected in series in order to increase the output voltage. Among the solutions found, we decided to include in our system the LTC3105, offered by Linear Technology for solar energy harvesting applications, which has low start-up voltage and includes a step-up DC/DC converter and maximum power point control [22]. We also considered other products from Texas Instruments, like the bq25504, but it has higher start-up voltage and is designed to charge a battery with the energy harvested from one single source [23], so the LTC seemed more complete and suitable for our multi-source application.

2.3 Harvesting energy from thermal sources

Thermal energy harvesters use temperature differences to generate power. They are based on the Seebeck effect, which states that when two different conductors at different temperatures are put together, a voltage appears between them. The simplest device based on this effect is a thermocouple (Figure 2.5), where the voltage is given by:

$$V = \alpha_1 \Delta T - \alpha_2 \Delta T$$

Where α_1 and α_2 are the Seebeck coefficients and depend on the material properties.

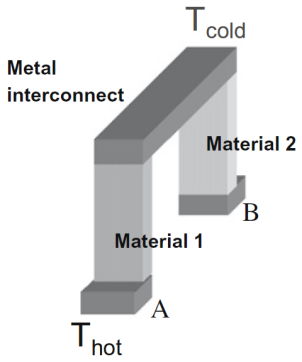

Figure 2.5: Schematic of a thermocouple [2]

The voltage generated by a thermocouple is usually low, particularly in micro-scale applications, where it is difficult to find and maintain large thermal gradients, especially due to the transducer's small size. However, several of them can be put thermally in parallel or electrically in series, creating a thermopile (Figure 2.6).

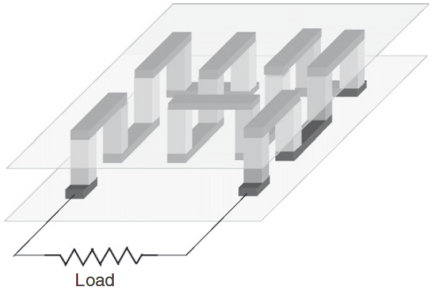

Figure 2.6: Schematic of a thermopile [2]

Anyway, sometimes it is possible to find differences of a few Kelvin between one surface and the other, or one surface and the air [2, 8, 10]. For instance, the thermoelectric transducer can be placed on the surface of a heat sink or a hot pipe, obtaining an adequate thermal gradient. In a larger scale, automotive companies such as Porsche are developing thermoelectric generators to be integrated into cars [24, 25].

Again, we will use a Linear Technology integrated circuit to increase the voltage given by the TEG. Both the LTC3108 and the LTC3109 are recommended for thermoelectric energy harvesting applications, but we chose the last one because it can operate from temperature differences of either polarity [26]. It operates from very low input voltages and includes a step-up converter and power management features.

2.4 Multi-source Energy Harvesting

Harvesting energy from one unique source is not usually a good strategy, due to its dependence on unpredictable environmental conditions. The best option is to combine it with an energy storage device, like a small battery or a supercapacitor, which will power the system when there is no ambient energy available, or when it is not enough to

provide peaks of power [2]. In addition, harvesting energy from several sources makes the system more reliable and ensures its long-term operation [27].

However, it is necessary that the system be able to manage different impedances and output voltages, as each harvester has its own characteristics. Modular energy harvesting systems, where each harvester works autonomously, can be a good answer for certain applications, but generally the best solution is to design a complementary balanced energy harvesting system, which ensures that the combination of the output power of all the harvesters is, at least, the power required by the system, while trying to minimize the harvesters' size [4].

There are a few works based on harvesting energy from various sources, but most of them are based on a modular system, where only the source with higher voltage is connected to the load, like in [28] or [27].

However, a MIT research team designed a system to harvest energy from light, thermal and vibration sources, and achieved higher efficiencies than previous works thanks to a dual-path implementation consisting in two separate converters for power management [29]. The current work aims to expand this design to a multi path topology.

Chapter 3

Energy Harvesting System Design

The energy harvesting system must include, at least, the following elements [10, 27]:

- One or more energy sources. Depending on the source, it will be necessary to convert the power before transferring it to the load or the energy storage device. Both the photovoltaic cell and the thermoelectric transducer generate continuous power, but the piezoelectric harvester outputs AC power, so an AC/DC converter is needed to rectify it. Moreover, if the voltage obtained is very low, we will need to raise it to the value required by the load with a boost converter.

- A circuit to maximize the energy obtained. For each harvester, there is a value of voltage that maximizes the output power, called the maximum power point (MPP). As we have said in Chapter 2, for photovoltaic cells this point has to be continuously tracked, as it depends on the light intensity, while for thermoelectric and piezoelectric transducers it can be tuned during installation because it does not change.

- A power management circuit, needed to protect the load and the batteries. For example, when there is no energy available in the environment, it prevents the battery from overdischarging. It also controls whether the load is powered by the energy harvesting source or the energy storage device.

- An energy storage device, to provide energy to the load when there is no ambient energy available. It can be a secondary (rechargeable) battery cell, a supercapacitor (EDLC) or other storage device. The technology chosen depends on the particular application and its demand of energy.

- A load or a system that we want to power. The output power will have to be adjusted to its needs. Buck and boost converters may be necessary to adapt the voltage from the storage device to the value required by the final load.

As we have explained in Chapter 2, energy harvested from the environment can be found in various sources: light, vibrations, thermal gradients, pressure gradients, RF... In our case, indoor light was chosen because our system is thought to be placed in a laboratory, and even though its power is much lower than the one of outdoor light, it is still a good option for low-power applications. Photovoltaic cells provide low level DC voltage, so their output must be increased to the level required by the load.

Harvesting energy from ambient vibrations has not been so investigated, but it has a big potential, due to the high energy available. As mentioned before, we decided that a piezoelectric transducer would the best option among the three mechanisms existing for vibration energy harvesting, because of its simplicity (no need of input voltage) and

performance. It must be taken into account that piezoelectric harvesters produce AC voltages that must be rectified, but they are relatively high so the voltage drop in the rectifier is generally acceptable.

Finally, we decided to include a thermoelectric generator too, in order to investigate this technology. Thermal gradients are relatively easy to find, but the challenge is to find differences big enough to produce significant power.

3.1 Energy harvesting Development Kit

After doing some research on existing energy harvesting applications and components, two alternatives were found. The first one consists of using a development kit, which includes a solar cell, a power management circuit, a microcontroller and a energy storage device. The second option consists of a customly designed energy harvesting system, choosing its components and assembling them. After comparing these options, we decided to start with a development kit because it would permit us to obtain results earlier, and moreover, a custom design is not required to benchmark the different harvesters and power path logic.

Several manufacturers, like Texas Instruments and Microchip, currently offer energy harvesting kits [30,31]. Both development kits are very similar, and they include a Cymbet evaluation board. In Table 3.1 there is a comparison between both boards, including their price via Farnell/Element14 distribution.

Table 3.1: Comparison between two energy harvesting development kits

Kit	Description	Microcontroller	Energy Storage Device	Price
Microchip	Microcontroller, LEDs, temperature sensor	PIC24F16KA102	Two thin-film batteries	84€
Texas Instruments	Microcontroller, LEDs	MSP430	Two thin-film batteries	158.63€

Finally, we chose Microchip's XLP 16-bit Energy Harvesting Development Kit, not only because it is considerably cheaper, but also because we considered that its microcontroller (PIC24F16KA102) is easier to program than the one of Texas Instruments (MSP430).

Microchip's development kit, shown in Figure 3.2, is an extremely low power platform specially designed for energy harvesting applications. The kit includes the following features:

- Cymbet solar energy harvester (CBC-EVAL-08). It incorporates an amorphous silicon solar cell, two 50 µAh EnerChip solid state energy storage devices and an energy harvesting Enerchip (CBC5300) that includes a boost converter and a power management circuit [32]. Figure 3.1 shows the block diagram of this kit.
- PICkit 3 debugger/programmer.
- Board elements such as LEDs, temperature sensors, potentiometer or EEPROM, which can be disabled by removing the appropriate jumper.

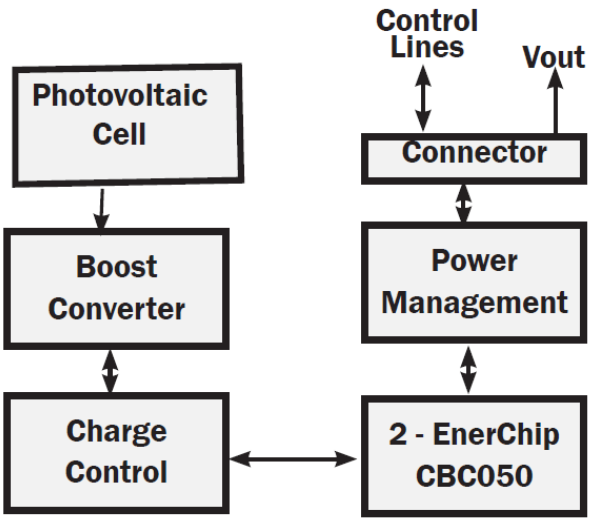

Figure 3.1: EnerChip EVAL-08 Demo Kit Block Diagram [32]

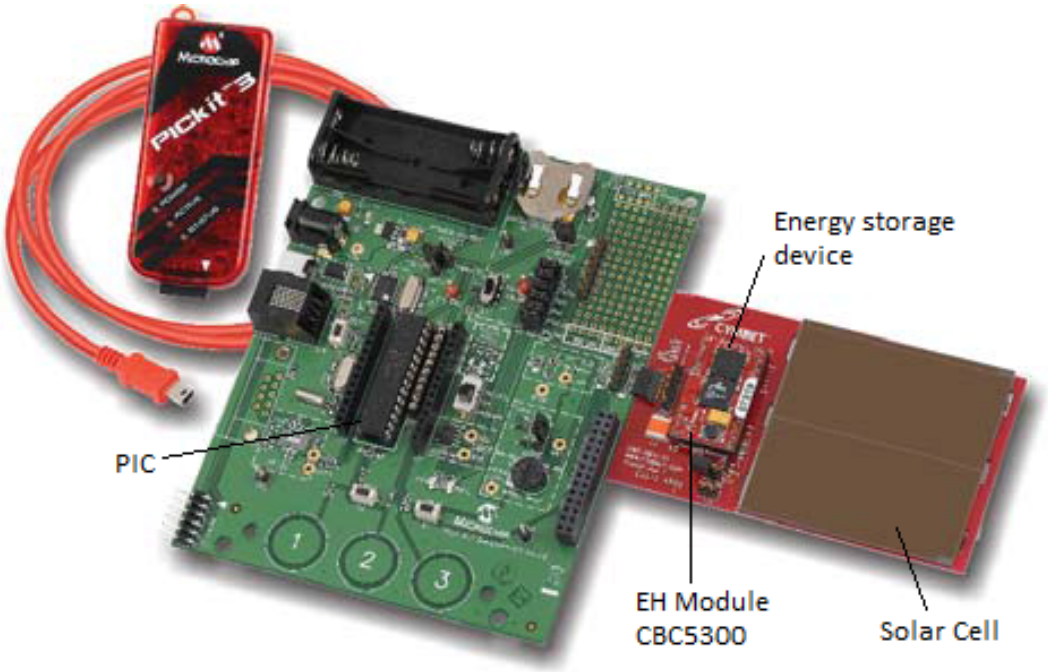

Figure 3.2: Microchip's XLP 16-bit Energy Harvesting Development Kit [30]

3.2 Piezoelectric Transducer

As we have said, we decided to use a piezo transducer to harvest energy from environmental vibrations.

Several piezoelectric manufacturers were reviewed, such as Piezo, Mide or Arveni, but finally a Mide transducer was chosen. Piezo's transducers seemed more complicated to connect to the board than Mide's ones, and Arveni's T-Rex appeared as a really good option because of its high efficiency, but it had strong frequency limitation (only suitable

for 50 Hz [33]).

Mide offers a wide variety of piezoelectric energy harvesters, and each one of them is addressed to a different range of frequencies. The main advantages of these harvesters are that they can be easily connected to other devices, and they can be tuned with a tip mass so that the natural frequency of the harvester is the same as the vibration frequency.

Mide Volture energy harvesters extract energy from environmental mechanical vibrations. To optimize the extraction, the product must be mounted in a cantilevered configuration and a tip mass must be added to vary the resonant frequency of the beam and make it equal to that of the vibration source, to obtain a maximal benefit from mechanical amplification.

As the frequency of the environmental vibrations is unknown, we selected three different energy harvesters, V22B, V21BL and V22BL (Figures 3.3, 3.4 and 3.5), each one addressed to a different range of frequencies. Each harvester includes two electrically isolated piezo wafers, which can be used independently, or can be connected in series or in parallel, depending on if double voltage or double current is needed [34].

Figure 3.3: V21BL

Figure 3.4: V22B

Figure 3.5: V22BL

As can be found in the datasheet [34], they all have the same thickness (0.79 mm) and operating and storage temperature range. However, the maximum output voltage, current and tip-to-tip displacement vary from one to another, as well as the range of frequencies they can deal with. The V22B is the shortest device, and it has the smallest tip-to-tip displacement, only 0.76 mm. V21BL and V22BL have similar lengths, and their tip-to-tip displacements are 4.57 mm and 3.05 mm respectively. Concerning the electrical characteristics, V22B and V22BL have identical series capacitance and resistance considering a single wafer. They have much higher resistance than the V21BL, but lower capacitance.

Moreover, the natural frequency ranges of V21BL and V22BL are similar. With no tip mass, the natural frequency is 110 Hz in both cases, but when adding a mass, it rapidly decreases for the V22BL. For instance, with a tip mass of 2 grams, the natural frequency is 30 Hz in the case of the V22BL, but it is between 50 and 65 Hz for the V21BL. The V22B is addressed to higher frequencies, given that its natural frequency is 240 Hz with no tip mass and it decreases until 80 Hz by adding 2 grams.

The open circuit voltage for a series connection of the wafers is higher for the V21BL, followed by the V22B, due to its lower series resistance. The characteristics of these devices can be summarised in the following table [34]:

Table 3.2: Characteristics of Mide Volture piezoelectric transducers

		V21BL	V22B	V22BL
Typical Thickness (mm)		0.79	0.79	0.79
Length (mm)		90.42	64.34	92.28
Operating Temperature Range		-40 - 90 °C	-40 - 90 °C	-40 - 90 °C
Storage Temperature Range		-60 - 90 °C	-60 - 90 °C	-60 - 90 °C
Maximum tip-to-tip displacement (in)		4.57	0.76	3.05
Single Wafer series capacitance (nF)	100 Hz	26	9	9
	120 Hz	26	9	9
Single Wafer series resistance (Ω)	100 Hz	950	2400	2400
	120 Hz	770	2000	2000
Natural Frequency (Hz)	Tip Mass 0g	110	240	110
	Tip Mass 1g	65	105	35
Price		51.98€	39.60€	39.60€

3.3 Thermoelectric Transducer

As mentioned before, thermoelectric transducers generate power from thermal gradients. After reviewing several manufacturers, we concluded that the best transducers for this application were those offered by Nextreme and Micropelt, due to their prices and output power for a given thermal difference. We chose Nextreme's eTEG HV37 (Figure 3.6) and Micropelt's TGP 651 (Figure 3.7). Their output voltage is very low, so it is necessary to increase it using a DC/DC step-up converter. Both thermoelectric transducers are designed for experimental applications, so we also acquired Marlow's EHA-PA1AN1-R02-L1, a thermal energy harvesting unit for industrial applications, which also includes a step-up converter and a heat sink, as can be seen in Figure 3.8.

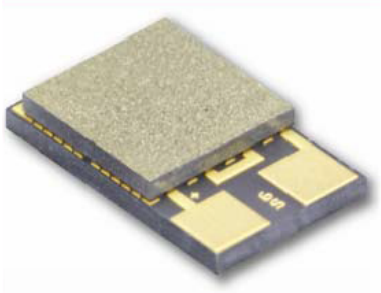

Figure 3.6: Nextreme eTEG HV37 [35]

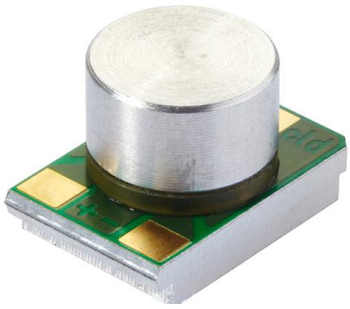

Figure 3.7: Micropelt TGP-651 [36]

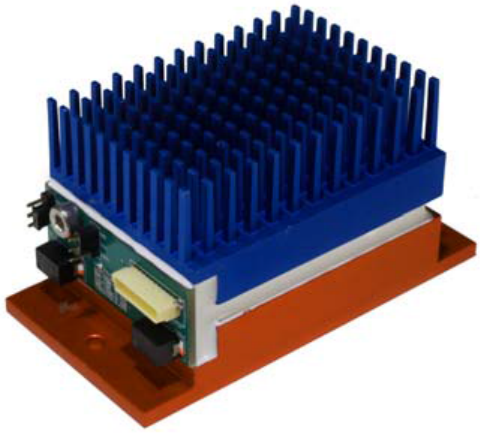

Figure 3.8: Marlow's Thermal EH Demo Unit [37]

Chapter 4

Starting with the XLP 16-bit Energy Harvesting Development Kit

The PIC24F microcontroller incorporated in the board is preprogrammed with a demonstration application where all the features included in the kit are used: LEDs, temperature sensors, low power modes... To get started with it, we followed the procedure described in the datasheet [38] to configure the hardware and software, and we tested its operation using RealTerm, a serial terminal program included in the kit, connecting the board to the PC via USB, as the firmware incorporates a USB-to-RS-232 converter. The demonstration application permits to change the low power mode or the sensor mode, and transmits real time information to the computer. Figure 4.1 shows a screenshot of the terminal program, where the measurements made and the low-power mode are indicated.

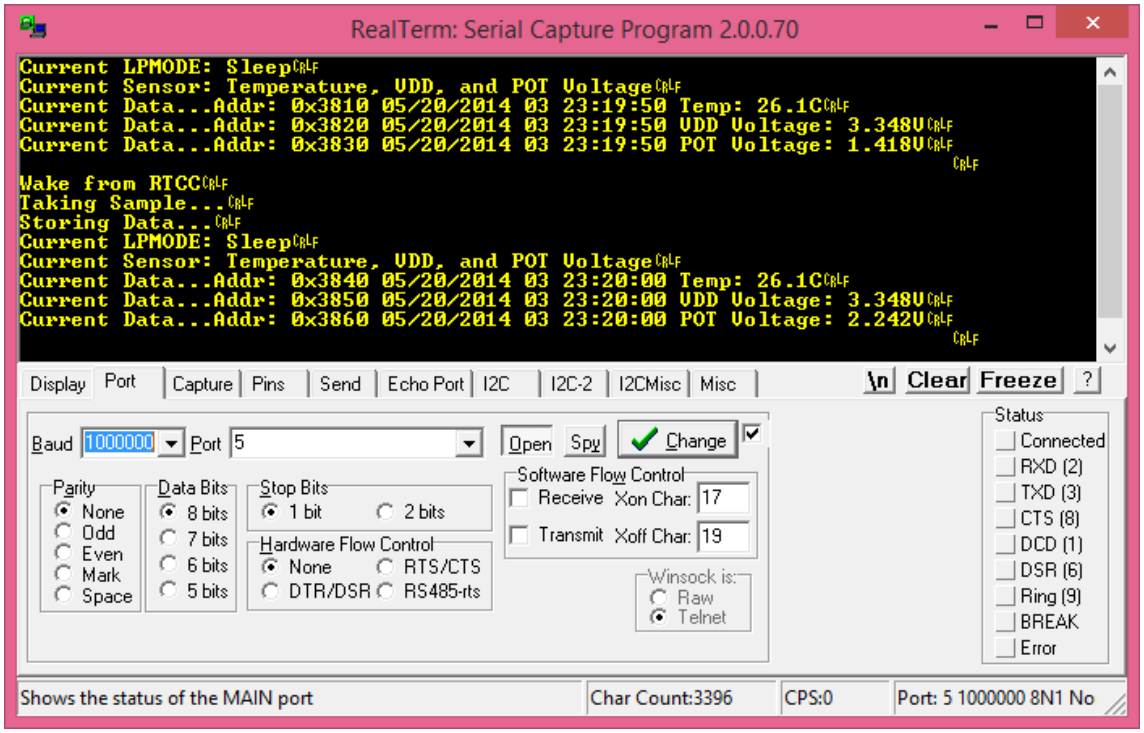

Figure 4.1: Realterm screenshot: demonstration application

Then, we connected the Cymbet solar harvester mentioned in Chapter 3 to Microchip's board using the interface headers. As specified in Microchip's board user guide [38], we changed the jumper to choose the energy harvester power source.

We also wanted to measure the voltage produced by the harvester, so we had to make a few modifications. We connected the header corresponding to Vout2 to an analog input of the microcontroller (AN10), configuring it in the code as an analog input, and defining a new function called *GetVoltVal*, to measure the voltage.

After connecting both boards, we observed that when the harvester source was selected, the board operated normally until a moment when brownout occurred, that is, the voltage was too low to guarantee normal operation, and it did not recover until the USB power source was selected. After analysing its behaviour, we found out that the battery voltage is usually 4,06 V (in microcontroller's Deep Sleep Mode), but when the Reset button is pressed, this voltage decreases because the microcontroller wakes up and demands energy from the Cymbet board to measure the sensors and send this information to the PC. If it is forced to do this very frequently, the battery voltage drops under a limit where it cannot recover anymore.

Obviously, the board operates in a different way depending on if there is light available or not. Covering the photovoltaic cell, it was observed that when the reset button is pressed and the output voltage drops below 3.2 V approximately, it cannot recover anymore unless the PV-cell is uncovered, that is, the cell starts providing energy.

Chapter 5

Parametrization of generator efficiency

Before starting to design the energy harvesting circuit, we need to know how much energy will be produced by the harvesters, in order to dimension the elements in the circuit.

The power produced by a generator, P_g, depends on multiple factors: the type of generator, its size, environmental conditions, environmental energy available, etc. Moreover, as the ambient energy is variable, P_g also depends on the time [4].

However, a simplification can be made by expressing P_g(t) as a function of three parameters, each one referring to a group of influencing factors: maximum normalized output power (p_g), size of the generator (μ_g) and efficiency (η_g).

The maximum amount of power that can be produced by the generator in optimal conditions depends on the materials used in the construction, the physical principles on which it is based and other technological parameters, which cannot be modified by the user. This value is usually specified by the manufacturer in the datasheet.

The size of the generator influences directly its performance, as generally bigger generators have higher efficiencies in power conversion, so the specific output power is a function of the size. This parameter can be chosen by the designer of the energy harvesting system.

Finally, the efficiency of the generator is determined by the environmental parameters, like changes in the ambient energy, so it is a function of the time and it cannot be modified by the user.

Using these three parameters, the maximum output power that can be produced by the generator can be expressed as:

$$P_g(t) = \mu_g p_g(\mu_g) \eta_g(t)$$

In the following sections we will parameterize the harvesters and we will explain the experiments done to calculate the real maximum output power.

5.1 Photovoltaic Panel

The photovoltaic cell included in Cymbet's board could not be connected because it is fixed to the board and internally connected to the energy harvesting module, so we analysed two different crystalline silicon solar cells. Thanks to the device and software that Davy Van Belle designed for his master thesis [39] (Figure 5.1), it is possible to obtain the maximum output power for a given light intensity and four different lamps: incandescent, halogen, LED and fluorescent.

By doing a sweep test we obtain a graph that represents the output for a range of light intensities, while the static test provides a graph with the U-I curve and the output power for a particular lamp and luminosity, indicating the maximum power point (MPP).

Figure 5.1: Testing device designed by Davy Van Belle

5.1.1 First panel

One of the photovoltaic panels (Figure 5.2) is a solar array composed by 4 cells, each one with a size of 2.5 $cm \times 5\ cm = 12.5\ cm^2$ [40].

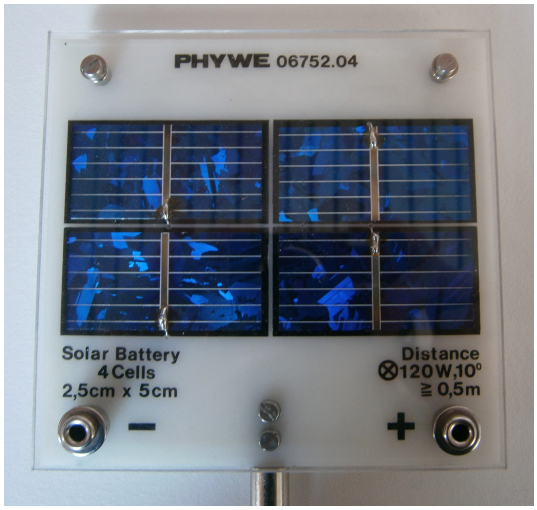

Figure 5.2: First photovoltaic cell

We made several sweep tests for the different lamps, but the results were very strange, with lots of peaks and no tendency, as can be seen in Figures 5.3 and 5.4. In addition, for the LED and fluorescent lamps, the program could not even show any graph.

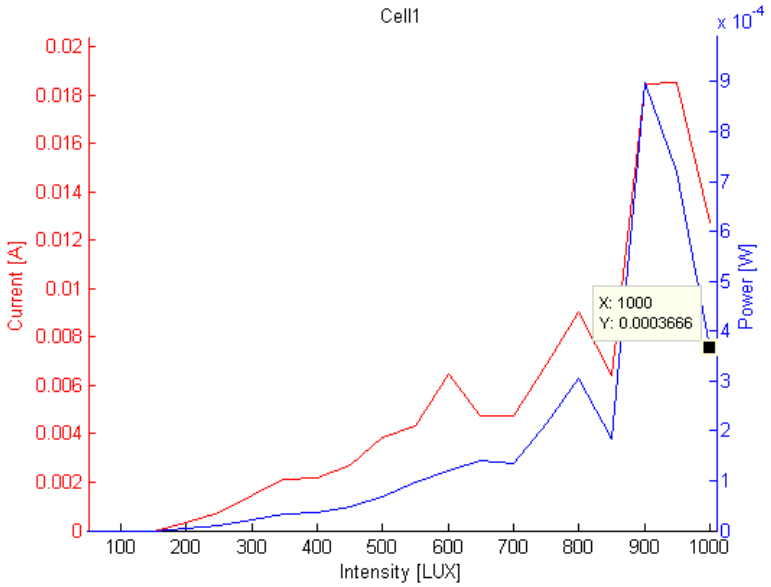

Figure 5.3: Output power and current for incandescent lamp (First cell)

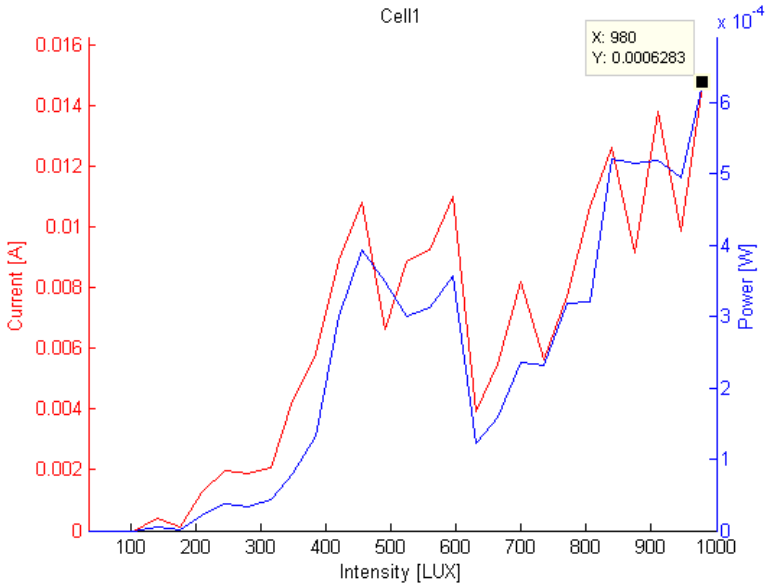

Figure 5.4: Output power and current for halogen lamp (First cell)

After repeating the tests with another cell of the same kind, we came to the conclusion that the cause of these results is probably the cells' degradation, as they have been stored for many years. A symptom of this degradation is that the conductors in the cells are oxidized. The fact that the cells are covered with a transparent screen could also contribute to the worse results.

5.1.2 Second panel

The other photovoltaic panel, shown in Figure 5.5, is composed by four cells of 2 x 6 cm^2 each, so $\mu = 2\ cm \times 6\ cm = 12\ cm^2$ per cell. Then, the total surface of the solar panel is $\mu_g = 48\ cm^2$.

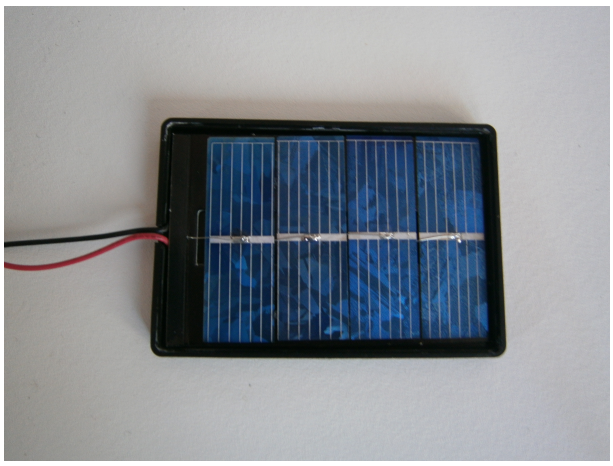

Figure 5.5: Second photovoltaic cell

The results for the sweep tests until a light intensity of 1000 lux are showned in Figures 5.6 - 5.9.

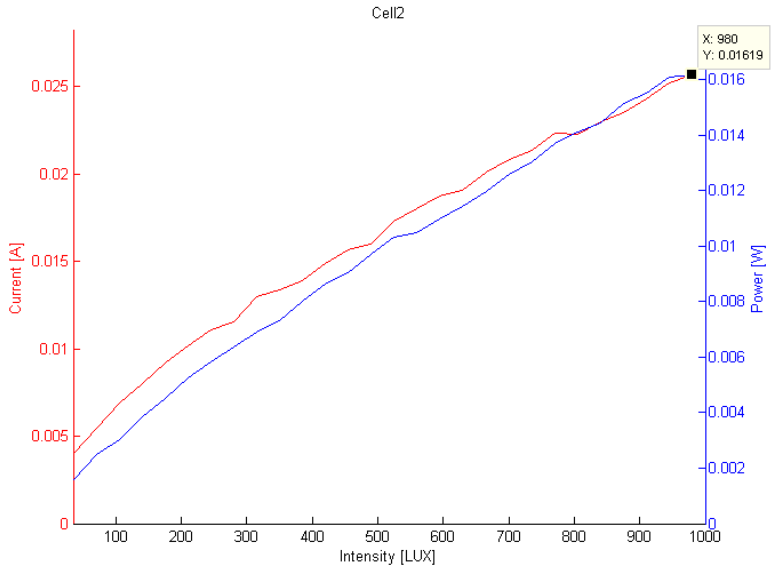

Figure 5.6: Output power and current for incandescent until 1000 lux (Second cell)

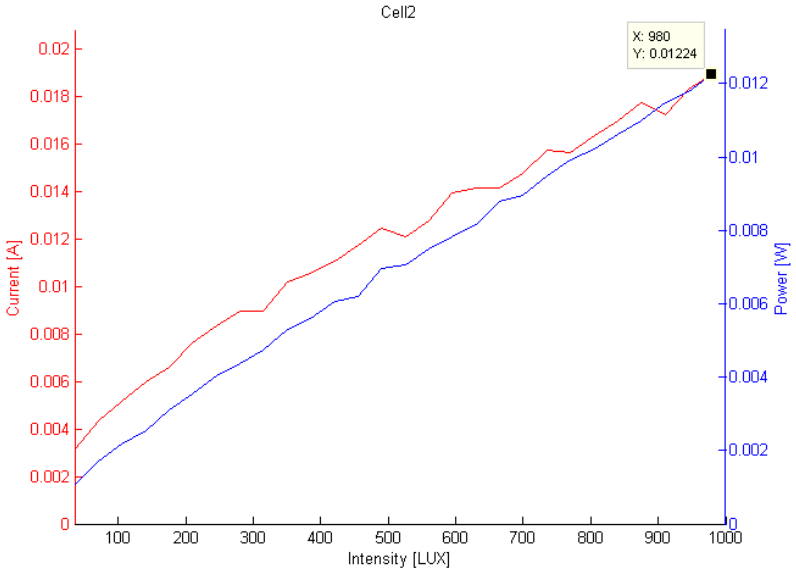

Figure 5.7: Output power and current for halogen lamp until 1000 lux (Second cell)

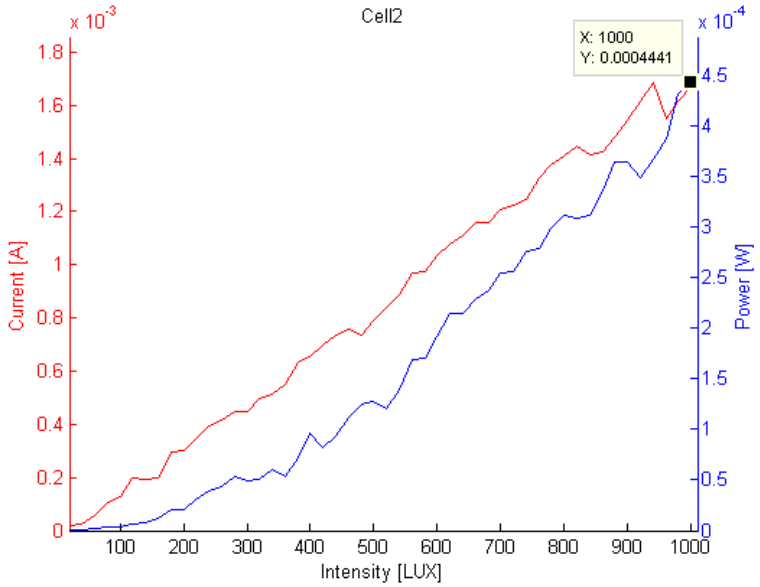

Figure 5.8: Output power and current for LED lamp until 1000 lux (Second cell)

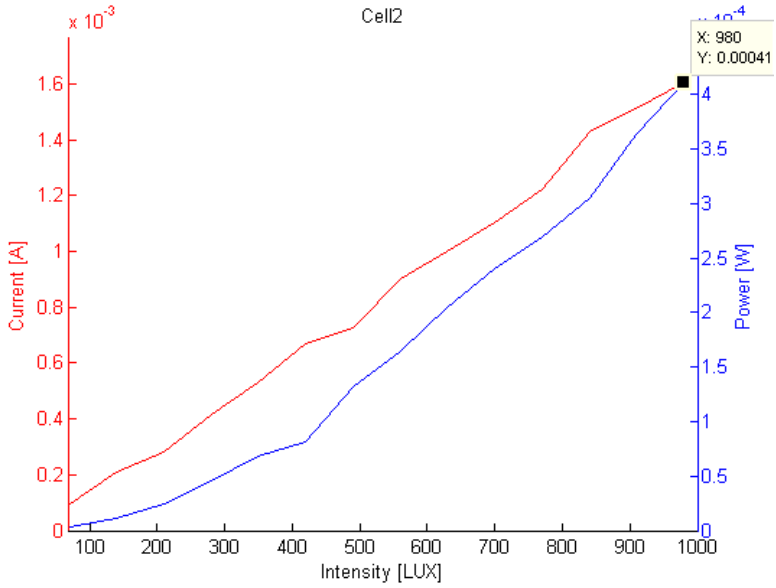

Figure 5.9: Output power and current for fluorescent lamp until 1000 lux (Second cell)

The results of the static tests made for the second cell for each lamp, at an intensity of 1000 lux, show that the output power is maximum for the incandescent lamp, as we can see in Figures 5.10 - 5.13. Given that we have no information about the theoretical maximum output power of this cell, we will consider that this value is the maximum at 1000 lux and in ideal conditions, and we will calculate the cell's efficiency for the other lamps based on this value.

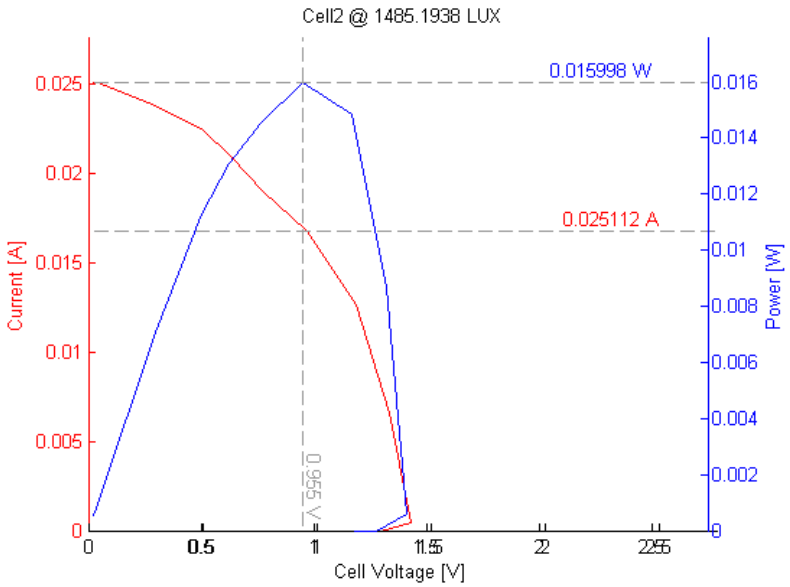

Figure 5.10: U-I and power curves at 1000 lux for incandescent lamp (Second cell)

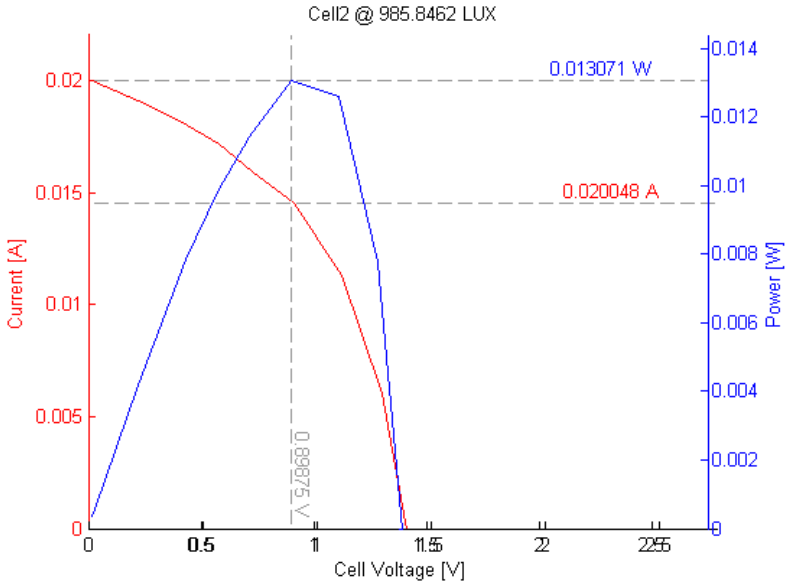

Figure 5.11: U-I and power curves at 1000 lux for halogen lamp (Second cell)

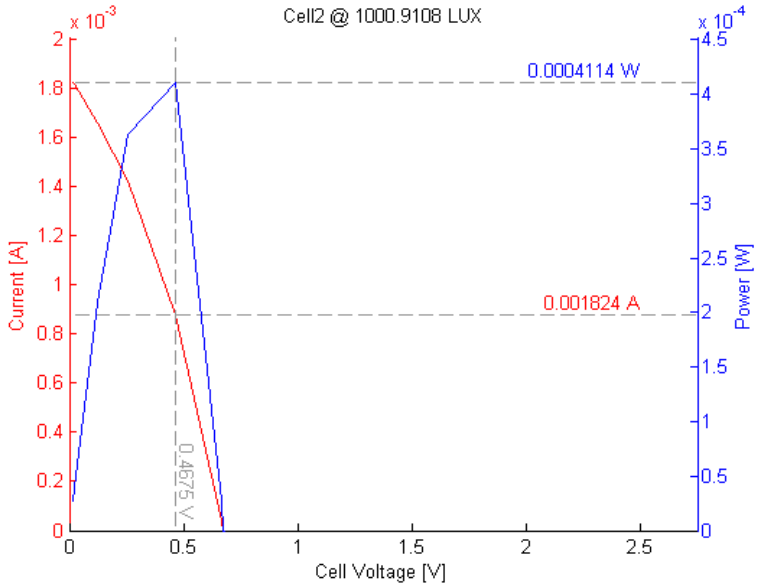

Figure 5.12: U-I and power curves at 1000 lux for LED lamp (Second cell)

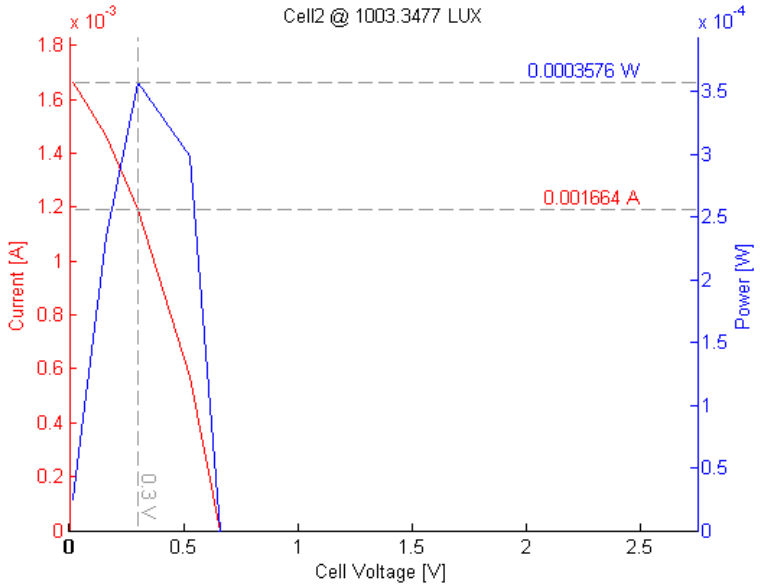

Figure 5.13: U-I and power curves at 1000 lux for fluorescent lamp (Second cell)

In the following table we summarize the results extracted from the graphs. As we have said before, the efficiency calculated in the table measures the performance of the cell for different kinds of lamps (not the light conversion efficiency), considering it maximum for the incandescent lamp. Although the MPP values (voltage and current) are given by the static tests, the ouput power is extracted from the sweep tests graphs at 980 lux because we consider that these values are more accurate.

Table 5.1: Output power and efficiency at 1000 lux for different lamps

Lamp	Voltage (V)	Current (A)	Power (W)	Efficiency(%)
Incandescent	0.955	0.025112	0.016019	100
Halogen	0.89875	0.020048	0.01224	76.41
LED	0.4675	0.001824	0.000431	2.69
Fluorescent	0.3	0.001664	0.00041	2.56

We can see that the cell is highly inefficient if we use a LED or a fluorescent lamp (less than 3%), while the efficiency if using a halogen lamp is very satisfactory. This results can be explained by the fact that incandescent and halogen lamps emit a continuous and broader spectrum of light.

If we repeat the test for a luminosity of 200 lux, which could correspond to a normal indoor light intensity, we obtain coherent results, as we can see in Figure 5.14. Lamp 2 corresponds to the incandescent lamp, Lamp 3 to the halogen lamp, Lamp 4 to the LED lamp and Lamp 5 to the fluorescent one.

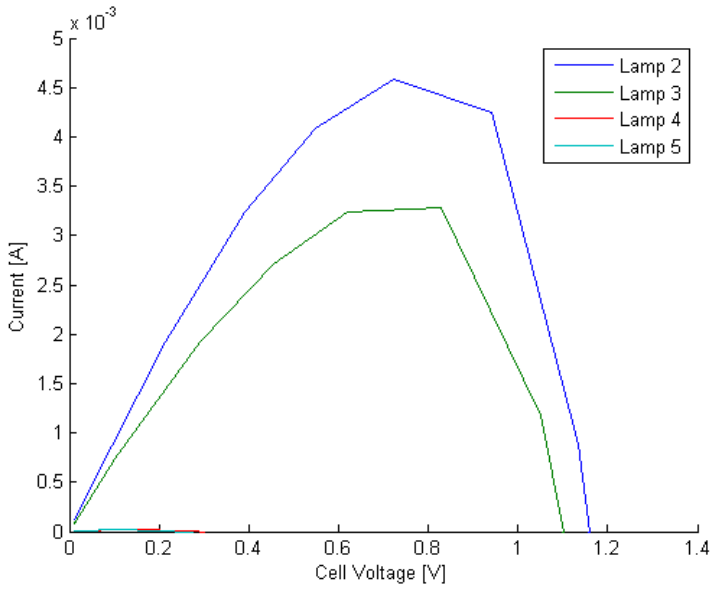

Figure 5.14: U-I curves at 200 lux for all lamps (Second cell)

5.2 Thermoelectric transducer

5.2.1 Nextreme eTEG HV37

In the datasheet of the Nextreme thermoelectric transducer [35] we can find that the maximum thermal difference at which it can operate is 200 K. The output power is given for thermal differences of 10 K, 50 K and 100 K, so we can estimate the maximum power that can be generated for a temperature difference of 200 K. Using a quadratic extrapolation, which is the one that best fits the values, we obtain that the maximum output power is 335 mW. Appart from the thermal difference, to achieve maximum power generation the output impedance must match the device resistance.

The data sheet also gives information about the dimensions of the harvester, so we can calculate its size:

$$\mu_g = 2.1\ mm \times 3.4\ mm \times 0.6\ mm = 4.284\ mm^3$$

Then, the normalized maximum generated power is:

$$p_g = \frac{335\ mW}{4.284\ mm^3} = 78.198\ mW/mm^3$$

To calculate the generator's efficiency we have to make some measurements of its output for different thermal gradients. Initially, we tried placing the harvester on a small hot plate but we did not obtain the results expected. The reason why it did not work is that there must be a constant heat flow through the TEG in order to maintain a constant thermal difference [41]. Then, we placed the TEG between the heat source and a heat sink with a fan incorporated, as shown in Figure 5.15, connecting them thermally with a thermal paste.

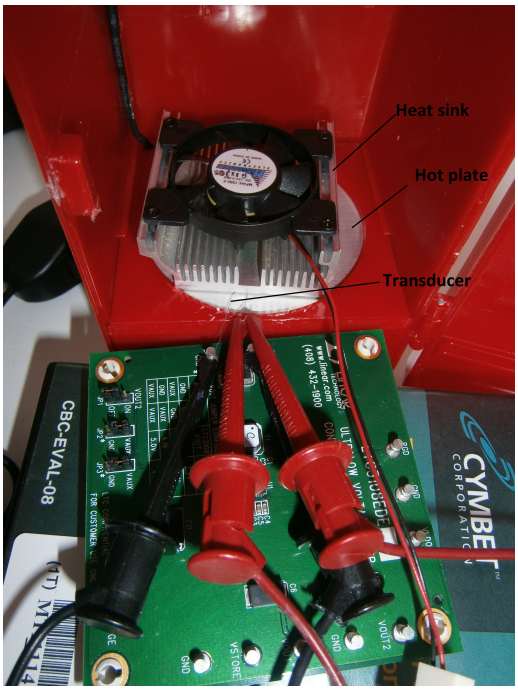

Figure 5.15: The system used to achieve temperature differences

Given the extremely small footprint of the harvester, it was impossible to measure the temperature in the cold and the hot side to calculate the real thermal gradient, so we measured the open-circuit voltage and calculated the temperature difference with the information given in the datasheet [35]. To measure the output current, we connected a variable resistor and adjusted it so that the harvester worked in the MPP, that is, when the output voltage is one half of the open-circuit voltage [29,35]. Figure 5.16 shows the relation between the measured output current and power, and the estimated thermal gradient.

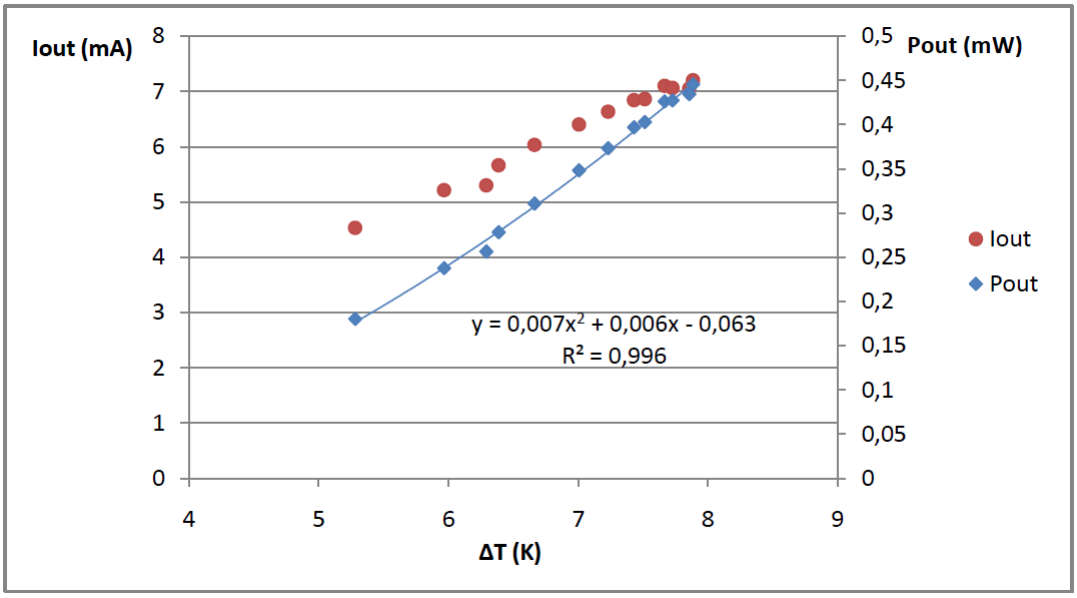

Figure 5.16: Output current and power against estimated thermal gradients

Using the regression curve, we can predict that the output power for a temperature difference of 200 K is 281.14 mW. Then, the efficiency of this harvester is:

$$\eta_g = \frac{281.14\ mW}{335\ mW} \times 100 = 83.92\%$$

Apparently, the Nextreme harvester has a really good efficiency. However, it must be taken into account that the temperature difference has been calculated with the datasheet, so it may differ from the real one, leading to a higher efficiency. Moreover, it is almost impossible to find such a big temperature difference in micro-scale applications.

5.2.2 Micropelt TGP-651

In the transducer's datasheet [36] we can find its dimensions to calculate its size:

$$\mu_g = 15\ mm \times 10\ mm \times 9.3\ mm = 1395\ mm^3$$

There we can also find a graph that represents the output power against the thermal gradient across the TEG. From the information given in this document we can suppose that the maximum thermal gradient to be applied is 60 °C, so we can extrapolate to calculate the maximum output power, which is $p_g = 21.72mW$. Then, the normalized output power for this device is:

$$p_g = \frac{21.72\ mW}{1395\ mm^3} = 0.016\ mW/mm^3$$

To measure the maximum output power, we used the same system that we used with the Nextreme harvester, composed by a small hot plate and a heat sink with a fan. As in that case, we measured the open-circuit voltage and then we adjusted a variable resistor to make the harvester work at the maximum power point, but we measured the thermal gradient by using two thin-film platinum temperature sensors.

At first, we tried placing one sensor between the TEG and the hot plate, and the other one between the TEG and the heat sink. However, the system was unstable and the

elements did not make good thermal contact, so finally we fixed the sensors with adhesive tape, one of them on the hot plate and the other one on the heat sink, trying to place them near the transducer, as can be seen in Figure 5.17. Figure 5.18 shows the results obtained from the experiment.

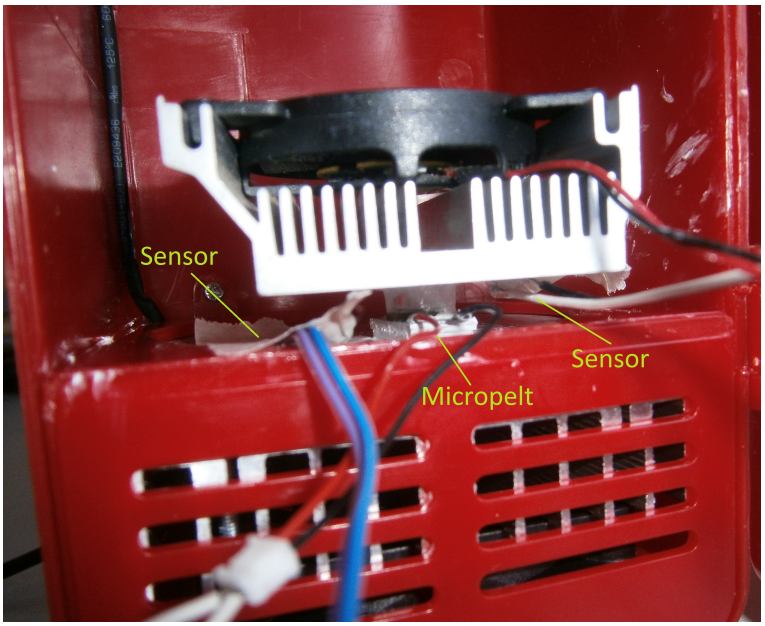

Figure 5.17: Setup to measure the temperature difference

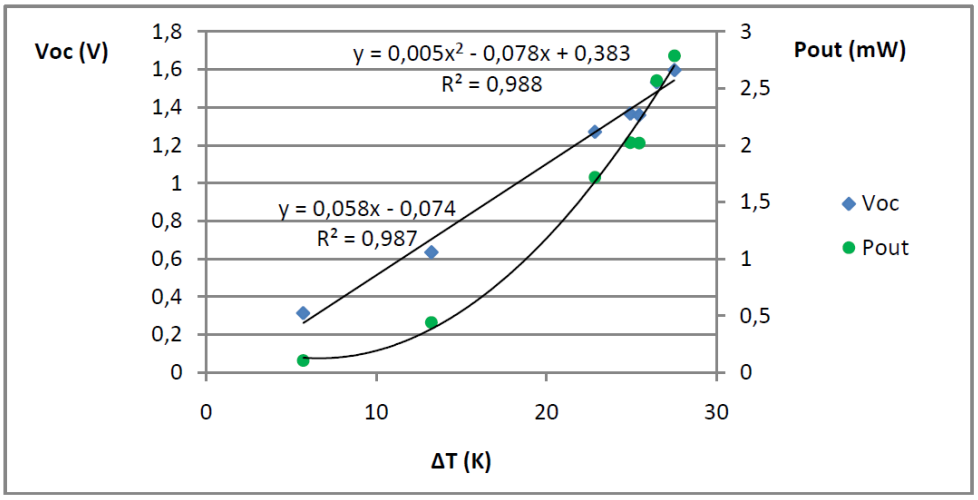

Figure 5.18: Open-circuit voltage and power for different thermal gradients

Due to the limited power of the hot plate, it was not possible to take more measurements, but the coefficient of determination is good enough to predict the maximum output power of the TEG. If we use the quadratic curve adjusted to the measurements, the estimated output power for a thermal difference of 60 K is 13.703 mW. Then, the generator's efficiency is:

$$\eta_g = \frac{13.703\ mW}{21.72\ mW} \times 100 = 63.09\%$$

5.2.3 Marlow EHA-PA1AN1-R02-L1

Marlow's energy harvesting unit harvests energy from thermal gradients between a warm surface and the ambient air. It already incorporates a heat sink and a step-up converter, as we have said in Chapter 3.

According to the datasheet [37], the size of the whole system is:

$$\mu_g = 38.1\ mm \times 74\ mm \times 38.2\ mm = 107701.08\ mm^3$$

From this document it is also extracted that the maximum temperature difference that can be applied to the system with no risk of damage is 60 K, and for this thermal gradient the maximum output power is said to be 2.3 mW, in the case where the selected output voltage is 5 V. Then, the maximum normalized output power is, in this case:

$$p_g = \frac{2.3\ mW}{107.7\ cm^3} = 0.021\ mW/cm^3$$

However, this maximum thermal gradient is calculated between the heat sink and the source, so there could be several degrees of difference between this value and the temperature difference across the TEG [37].

We can easily make measurements thanks to the wire harness included in the kit, where we can measure the output voltage and the temperatures at the hot side and the cold side of the TEG by reading the thermistors resistance and converting it with the formula given in the datasheet. For the experiment, we used a ceramic power resistor of 10 W as heat source and we applied different levels of power using a DC power supply to achieve various thermal gradients. We also put thermal paste between the resistor and the system in order to connect them thermally, and we connected a variable resistor to the system output.

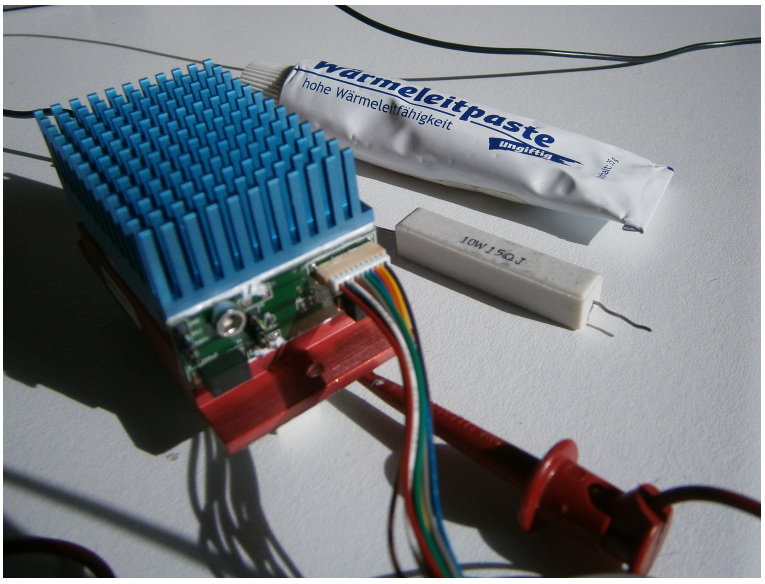

Figure 5.19: Marlow's unit with the wire harness and the power resistor used

As the output voltage is measured at the output of the LTC3108, it is constant until the load requires too much current, when it drops. So, in order to calculate the maximum output power, we connected a variable load (potentiometer) and we varied its resistance until the voltage decreased. Measuring the minimum load value for which the unit still outputs 5 V, we can calculate the maximum output current and then, the maximum

output power. Figure 5.20 shows the relation between the maximum output power and the thermal gradient across the TEG.

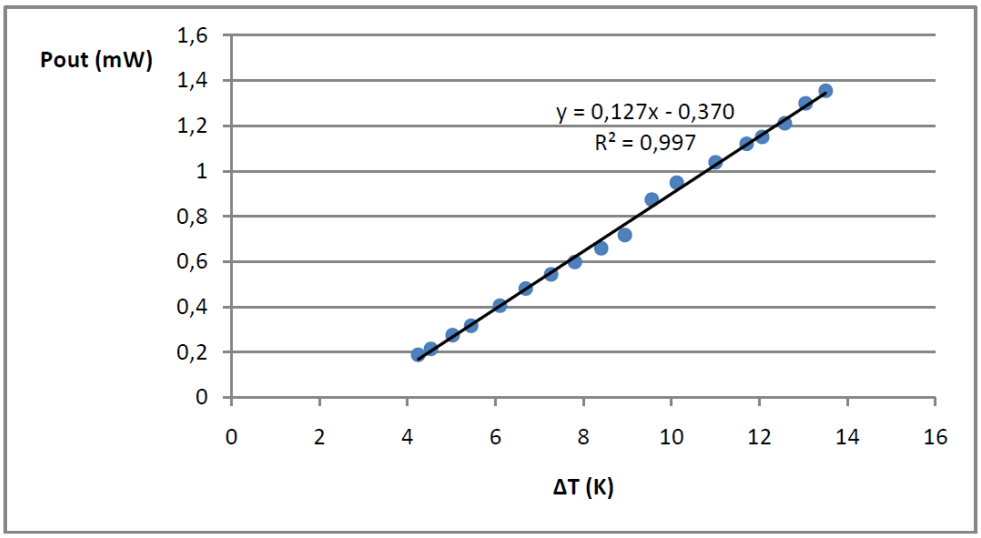

Figure 5.20: Maximum output power in function of the temperature difference

As we can observe in the graph above, the relation between the temperature difference and the output power is linear. If we extrapolate the regression curve, we obtain that the output power is zero for thermal gradients below 2.9 K. In the datasheet [37] it is said that the minimum temperature difference is 5.5 Kelvin, but it is calculated between the hot and the cold surface of the whole system, so the result we have obtained is valid, as we are measuring the temperature difference across the TEG.

In order to prevent damage of the transducer we kept the thermal gradient under 14 K, when the temperature in the power resistor, measured with a laser, was around 70 °C. For a thermal gradient of 13.5 K the maximum output power was 1.35 mW. If we compare this value with the one given in the datasheet, we have that the generator's efficiency is:

$$\eta_g = \frac{1.35\ mW}{2.3\ mW} \times 100 = 58.9\%$$

For benchmarking purpose, we also wanted to measure the maximum amount of current that could be delivered, so we followed the procedure indicated in page 4 of the datasheet [37] to measure the short-circuit current. For a load of 200 Ω and a temperature difference of 14 K (across the TEG) the output current was 381.9 μA. Then, for a constant thermal gradient, we varied the load resistance from 1 Ω to 1100 Ω, obtaining the graph in Figure 5.21.

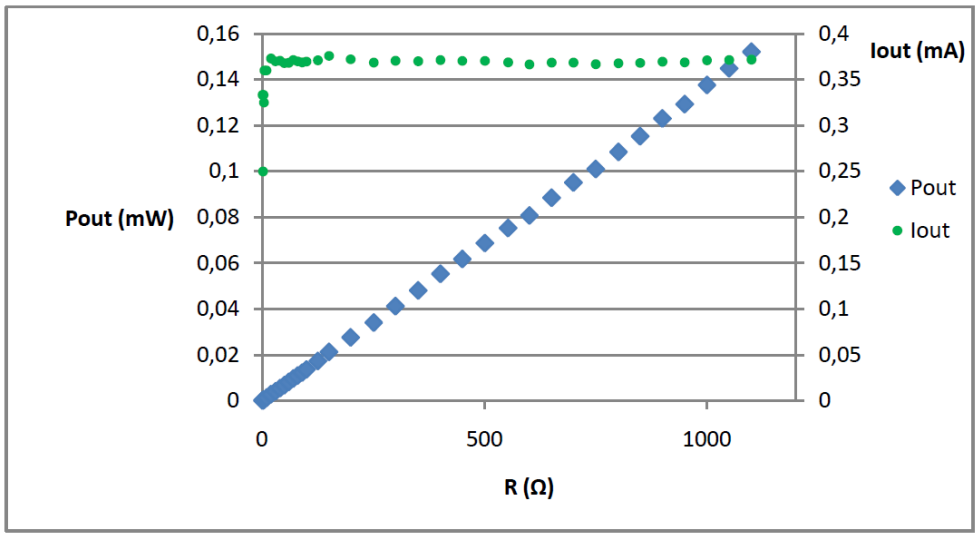

Figure 5.21: Output current and power for different loads

As we can see in the graph, the current is more or less constant, as the system is providing maximum current. Finally, we measured the output for an arbitrary load, to obtain the response for a constant load and different temperature differences across the TEG. For a resistance of 1500 Ω we obtained the results in Figure 5.22.

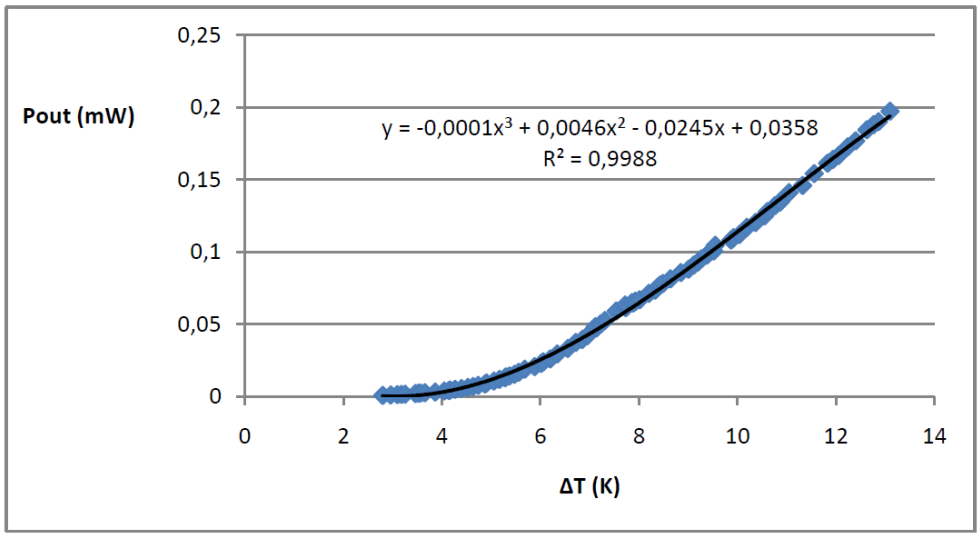

Figure 5.22: Output power against thermal gradient for a constant load

If we just consider the data from a temperature difference of 5 K, we can see that the relation between the output power and the temperature difference is linear, as shown in the datasheet.

5.3 Piezoelectric transducer

The dimensions of the different models of piezoelectric transducers can be found at Mide datasheet [34]. The sizes are:

V21BL	3.310 in x 0.660 in x 0.031 in = 0.068 in^3 = 1.449 mm^3
V22B	2.283 in x 0.600 in x 0.031 in = 0.042 in^3 = 0.909 mm^3
V22BL	3.383 in x 0.600 in x 0.031 in = 0.063 in^3 = 1.347 mm^3

The maximum output power is not given directly. Its value depends on the harvester model, the characteristics of the vibration and the tip mass used. However, the datasheet includes some graphs for each transducer, from which we can estimate the maximum generated power.

With the piezo wafers connected in series, the transducer V21BL generates 2.662 mW for a vibration of 40 Hz and amplitude 1 g, when a tip mass of 4.8 grams is used. The V22B can produce 0.59 mW with a tip mass of 2 grams, and a vibration of 80 Hz and 1 g of amplitude. Finally, the V22BL generates 1.84 mW from a vibration of 30 Hz and 1 g of amplitude, with a tip mass of 2 grams.

In order to characterise the performance of the different piezoelectric harvesters, we have to measure their output for different loads, tip masses and vibrations. At first, we tried placing the harvester on a speaker and connecting it to a signal generator (Figure 5.23). However, the open-circuit voltage of the piezo harvester was in the order of milivolts.

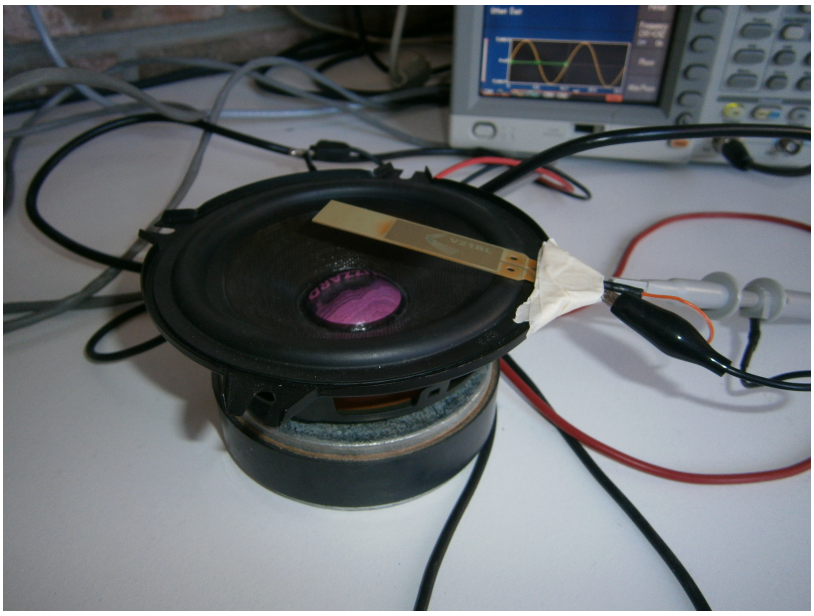

Figure 5.23: Using a speaker as a shaker

According to the datasheet [34], this bad performance could be due to an improper attaching and clamping of the harvester. For instance, the base where we clamp the transducer should be made of a rigid material, while the speaker's surface is elastic. Then, we decided to build a structure similar to the one used in [42], which is composed by a speaker, a wave generator and a platform where the piezo harvester is fixed in a cantilevered configuration. Figure 5.24 shows the implemented system; we 3D-printed a plastic tube, and we glued the speaker, the tube and a MDF board, where we fixed the harvesters. The V21BL was clamped using screws and washers, as it has two holes for this purpose, while the V22B and V22BL were fixed with threads.

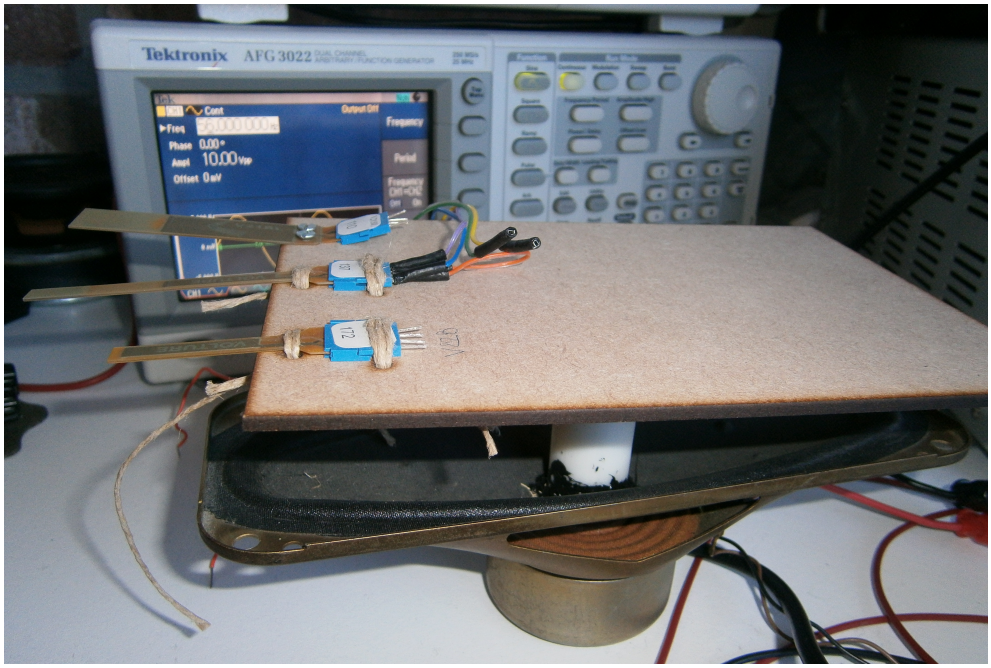

Figure 5.24: Structure built to fix the piezoelectric harvesters

Using this system we obtained better results than before, that is, the open-circuit voltage with the wafers connected in series was in the order of a few volts. To tune the harvesters, we made a frequency sweep to find when the open-circuit voltage was maximum. For example, Figures 5.25 and 5.26 show the open-circuit voltage of the V21BL for two different frequencies, using a tip mass of 4.8 grams. In this case, the natural frequency of the harvester is 50 Hz, and we can appreciate that the voltage is much higher at this frequency than at 55 Hz, although there is a difference of only 5 Hz. We repeated this procedure for the three harvesters and for different tip masses, obtaining the results in Table 5.2.

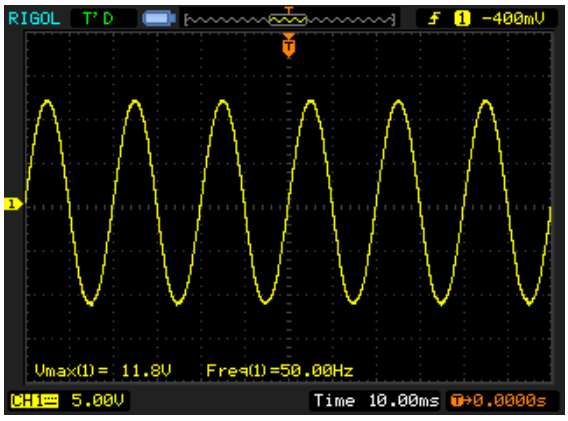

Figure 5.25: V21BL open-circuit voltage at 50 Hz (4.8 grams)

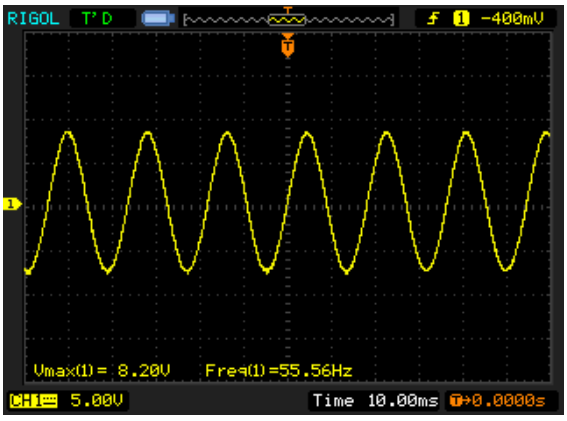

Figure 5.26: V21BL open-circuit voltage at 55 Hz (4.8 grams)

Table 5.2: Piezoelectric Harvesters' Natural frequencies for different tip masses

Product	Tip Mass (g)	Natural Frequency (Hz)	Open-circuit Voltage (V)
V21BL	0	205	5.6
	1	75	10.4
	2.4	59	10
	4.8	50	11.4
V22BL	0	58	2.8
	0.5	36	4
	1	34	2.6
	2	36	2.2
V22B	0	217	3
	0.5	215	3
	1	56	3.2
	2	56	2.8

These results are very different from the values given in the datasheet, especially for the harvesters V22BL and V22B, probably due to their worse clamping. Other reasons can be that the system that we are using affects the natural frequency of the harvesters, and that the amplitude of the vibrations that we are applying is very different from the one used in the datasheet. We tried to measure this amplitude by placing an accelerometer next to the transducers, as can be seen in Figure 5.27, but adding this element to the platform changed the natural frequency and decreased the open-circuit voltage.

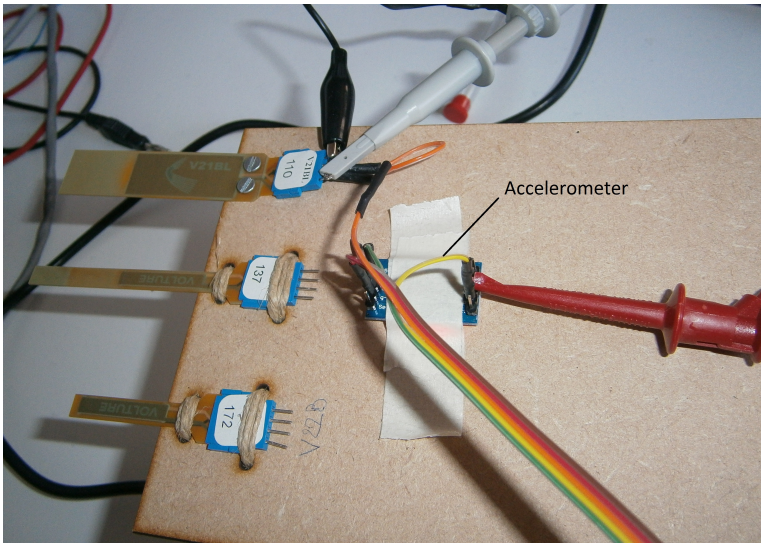

Figure 5.27: Setup including an accelerometer to measure the amplitude of the vibration

To calculate the maximum output power, we connected several loads, from 1 KΩ to 2.2 MΩ, to measure the output voltage. Figures 5.28 - 5.30 show the results obtained.

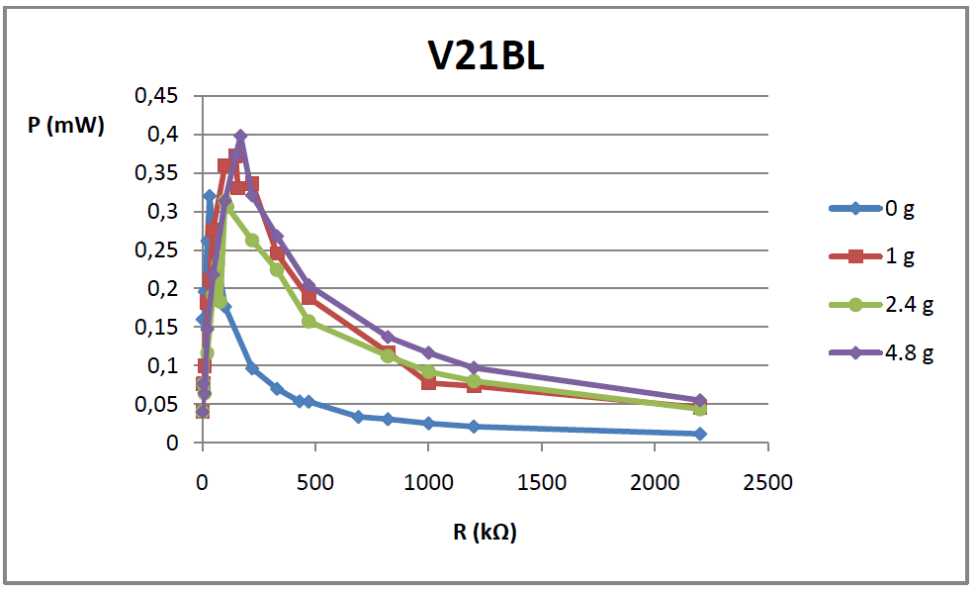

Figure 5.28: Output power from V21BL harvester for different loads

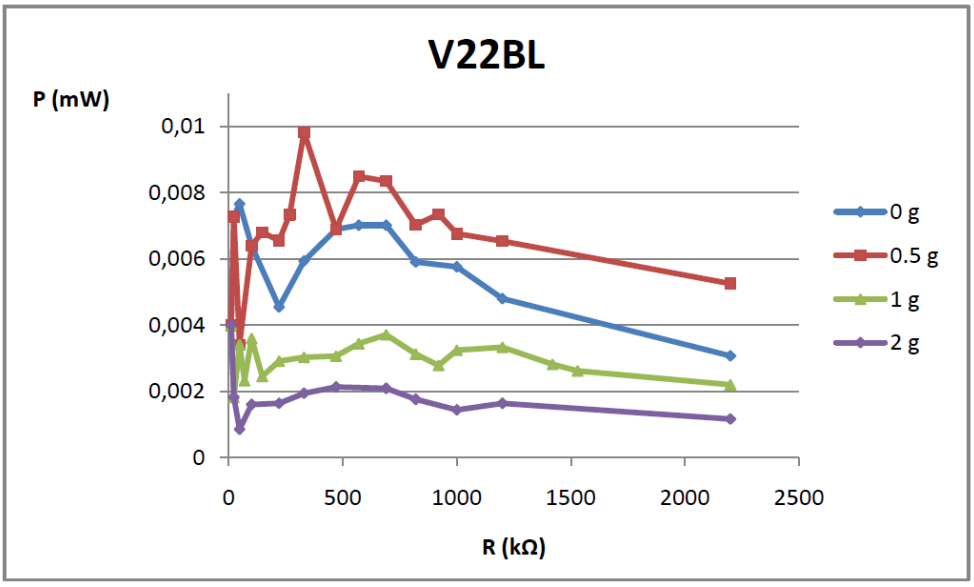

Figure 5.29: Output power from V22BL harvester for different loads

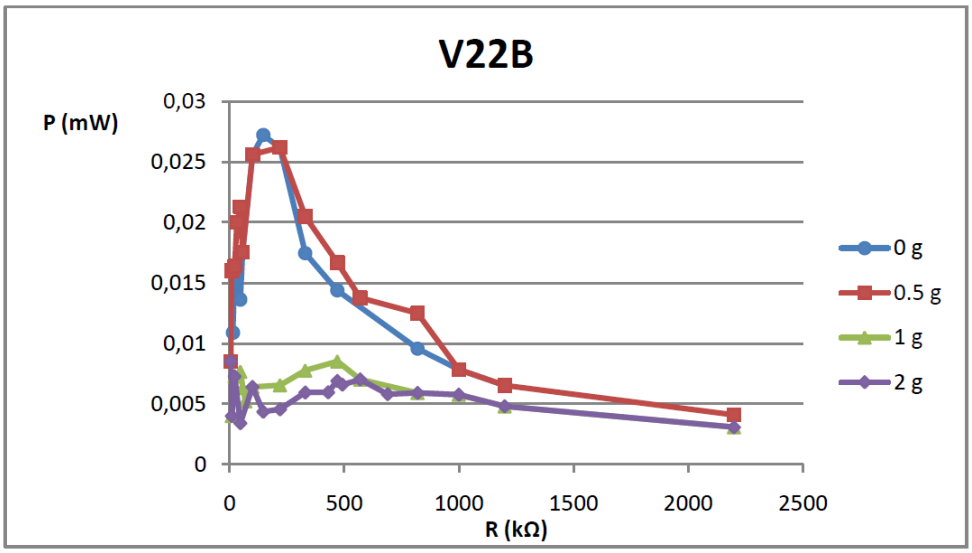

Figure 5.30: Output power from V22B harvester for different loads

In these graphs we can see that there is a resistor value for which the output power is maximum (MPP). If we compare these power values with the ones given in the datasheet we can see that they are much lower. Moreover, the output power should be higher for bigger tip masses, but using the V22BL (Figure 5.29) and the V22B (Figure 5.30) it is not like that. However, we have already seen in Table 5.2 that, for these transducers, the open-circuit voltage hardly changed when adding a tip mass, so we could expect a strange behaviour.

The maximum output power is obtained with the V21BL, tuned to 50 Hz and using a tip mass of 4.8 grams, and its value is 0.4 mW for a load of 169 kΩ. There is no point in calculating the efficiency of this harvesters, as we have not made the measurements in the same conditions as they were made in the datasheet. We can conclude that the system built permits to obtain relatively high output voltages, but it is still far from ideal. Moreover, it has been observed that the performance depends too much on the test setup.

5.4 Summary and conclusions

In Table 5.3 we can find a summary of the results obtained for the different harvesters. There is a huge difference between the Nextreme and the rest of harvesters, but this output power has been calculated for a thermal difference of 200 K, which is almost impossible to achieve in micro-scale applications. Then, the PV-cell is the harvester that outputs more power, followed by the other thermoelectric transducers, but again their outputs have been calculated in optimal conditions.

Table 5.3: Maximum output power for different energy sources and harvesters

Energy source	Harvester	Maximum output power (mW)	Conditions
Indoor light	Photovoltaic Panel	16.02	Incandescent lamp, 1000 lux
		12.24	Halogen lamp, 1000 lux
		0.43	LED lamp, 1000 lux
		0.41	Fluorescent lamp, 1000 lux
Temperature difference	Nextreme	281.14	$\Delta T = 200$ K
	Micropelt	13.70	$\Delta T = 60$ K
	Marlow	1.35	$\Delta T = 13.5$ K
Vibrations	Volture V21BL	0.40	Tuned with a tip mass of 4.8 grams
	Volture V22B	0.03	Tuned with a tip mass of 0 gram
	Volture V22BL	0.01	Tuned with a tip mass of 0.5 grams

Chapter 6

Power Path Management

6.1 Power Path Design

Once we have parameterized all the harvesters, our goal is to implement a system that combines the energy provided by each of them in an efficient way, that is, a complementary balanced energy harvesting system. This system has to be able to power a load (or charge a battery) with the energy from all the sources at the same time, not only from the one that is providing more energy at that moment, as it has been done in previous works [27, 28].

The system designed can be divided in four different parts: the solar energy harvesting circuit, the piezoelectric energy harvesting circuit, the thermoelectric energy harvesting circuit and the battery charging circuit. At the output of each energy harvesting circuit, there will be a capacitor to temporally store the energy harvested from each individual source, and there will be a final capacitor that will store the energy provided by the three circuits. The output capacitors for the energy harvesting circuits need to be able to store, at least, the energy produced in a few pulses of the corresponding switching regulator. All the capacitors will be of 10 μF, except from the final one, which will be of 100 μF, as it needs to store more energy.

Given that each capacitor will be at different voltage, depending on the energy available at the corresponding source, we will place some transistors to regulate the energy transfer, all of them controlled by the microcontroller. Figure 6.1 shows an schematic diagram of the system.

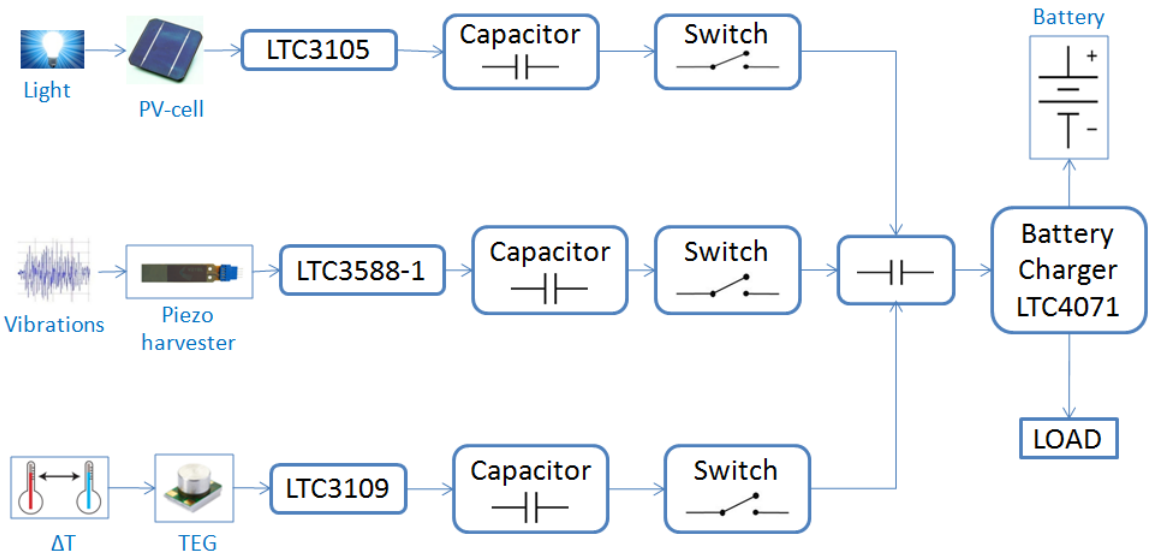

Figure 6.1: Schematic diagram of the circuit designed

In the following sections we will describe in detail each part of the circuit and explain how it works. The whole circuit is represented in Figure 6.10.

6.1.1 Solar Energy Harvesting System

As it was seen in Chapter 5, indoor photovoltaic cells provide low voltages, so their output has to be increased to power a load. For this purpose, we use the LTC3105 integrated circuit, which includes a step-up converter and maximum power point control, and it operates from low input voltages [22], as it has been mentioned in Chapter 2. We implement the circuit appeared in page 1 of the datasheet, making a few changes. At its output, we implement a boost topology, composed by an inductor, a MOSFET and a diode, to charge the capacitor when there is energy available.

The LTC3105 also includes a feedback pin used to regulate the output voltage. The block diagram appeared in the datasheet [22] shows that the voltage measured at this pin is compared to 1.004 V in order to control the step-up converter, so in order to guarantee that the voltage measured will be around 1 V, we put a resistor divider with a zener diode in parallel. When the voltage drop in the diode is 2.4 V, the voltage in the feedback pin will be 1 V.

Figure 6.2 shows the schematic circuit of this part of the system, including the final MOSFET transistor that regulates the energy transfer.

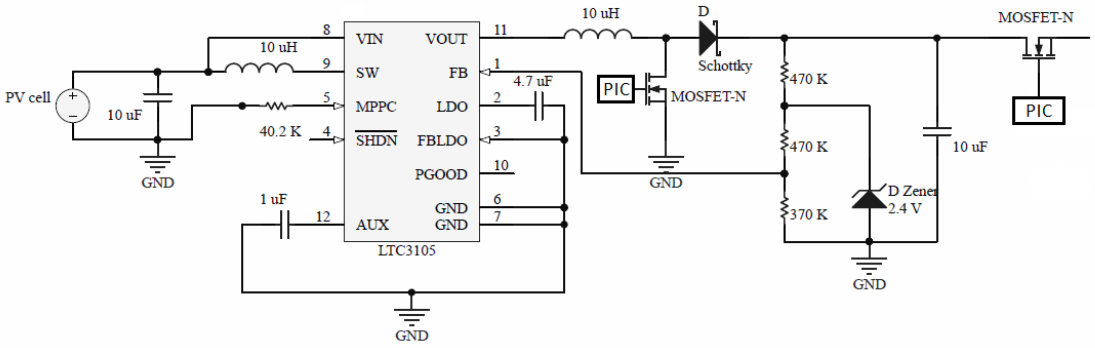

Figure 6.2: Solar energy harvesting circuit

6.1.2 Piezoelectric Energy Harvesting System

As it has been said in previous chapters, piezoelectric harvesters supply AC power. To rectify it, we use the LTC3588-1, as it incorporates a full-wave bridge rectifier and a buck converter [15], and we connect to the Switch pin of the chip the same boost topology used for the solar energy harvesting system, as can be seen in Figure 6.3. In this case, the output voltage is fixed using pins D0 and D1, and the feedback pin used to regulate the output is Vout. The LTC3588-1 has four selectable output voltages, so we choose one of this values (3.6 V) and we connect the feedback pin so that the output is regulated, regardless of the voltage in the output capacitor. With the zener diode connected to the Vout pin, we make sure that even if the voltage in the capacitor is big, the voltage monitored will not be greater than 3.6 V, and the circuit will not tend to decrease it.

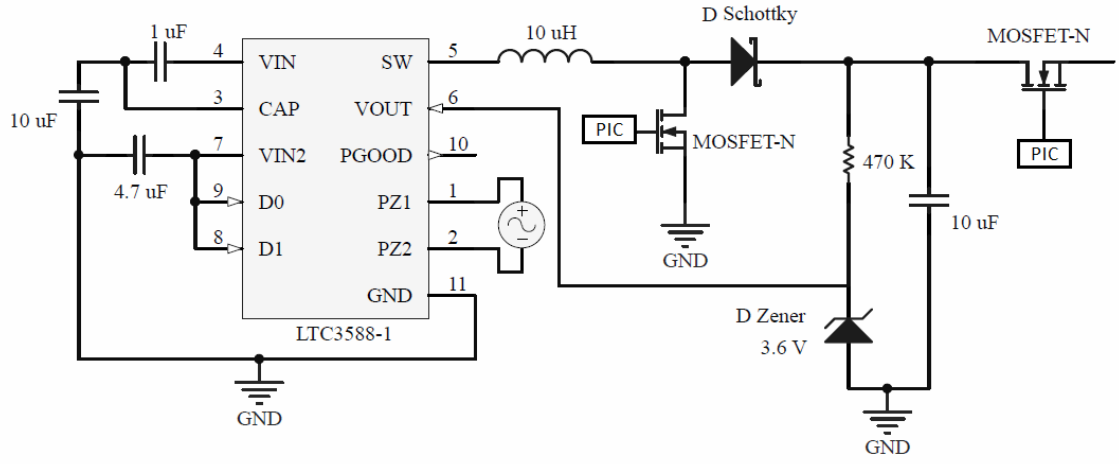

Figure 6.3: Piezoelectric energy harvesting circuit

6.1.3 Thermoelectric Energy Harvesting System

In order to increase the voltage supplied by the thermoelectric generator, we use the LTC3109. As it has been said in Chapter 2, it operates from very low input voltages, and it can be configured to operate from temperature differentials of either polarity [26]. This chip also has four selectable output voltages, configured with pins VS1 and VS2 (Table 6.1), but it does not include a feedback pin. As the voltage in the output capacitor

will vary, it is not suitable to fix the output voltage and connect the capacitor to this pin, because if the voltage in the capacitor is higher than the output voltage, it will not be charged and we will be wasting energy. In order to solve this problem, we decided to include a logic circuit, represented in Figure 6.4, that will select the output voltage value depending on the voltage of the output capacitor.

Table 6.1: LTC3109 Output voltage configuration [26]

VS1	VS2	V_{OUT}
0	0	2.35 V
0	1	3.3 V
1	0	4.1 V
1	1	5 V

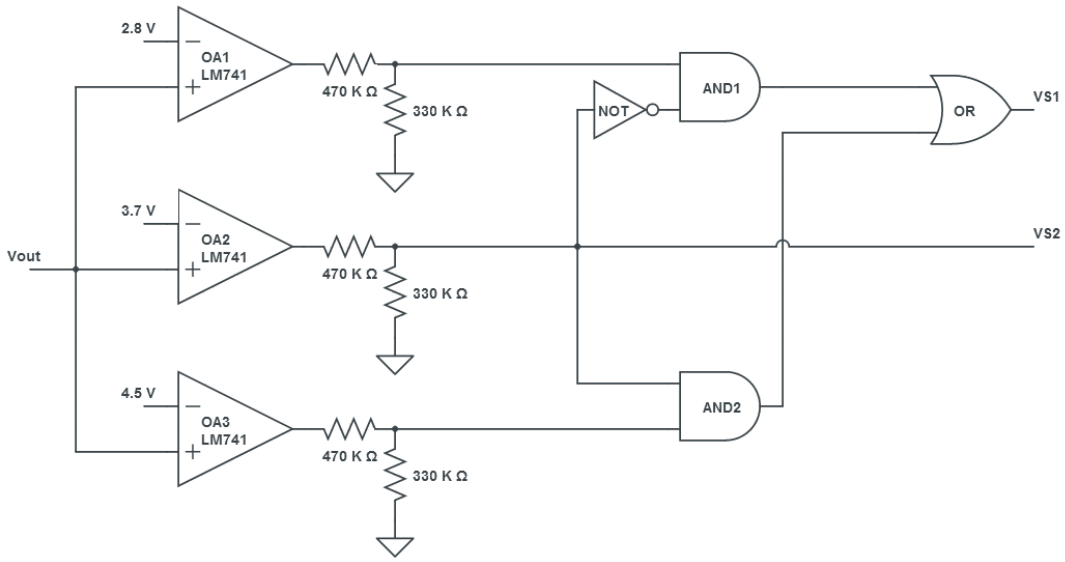

Figure 6.4: Logic circuit implemented to select the output voltage

This circuit is composed by three operational amplifiers (LM741) that compare the voltage of the capacitor with some reference values, and their outputs are connected to some logic gates to produce the correct voltage for pins VS1 and VS2. If the voltage of the capacitor is below 2.8V, the circuit will select an output voltage of 2.35 V. If it is between 2.8 V and 3.7 V, it will configure the output to 3.3 V. If the voltage is between 3.7 V and 4.5 V, V_{OUT} will be configured to 4.1 V. And finally, if the voltage of the capacitor is above 4.5 V, the output voltage will be 5 V. These operational amplifiers could be replaced by the MCP601 (Microchip), more suitable for this application, as it is a low-power op amp with a single supply from 2.7 V [43], so it could be powered from the same source as the PIC.

Moreover, we configure the circuit to work with temperature differences of both polarities, as indicated in the datasheet [26], and we implement at the output the same

boost topology used before. The thermoelectic energy harvesting circuit, excluding the logic part, is represented in Figure 6.5.

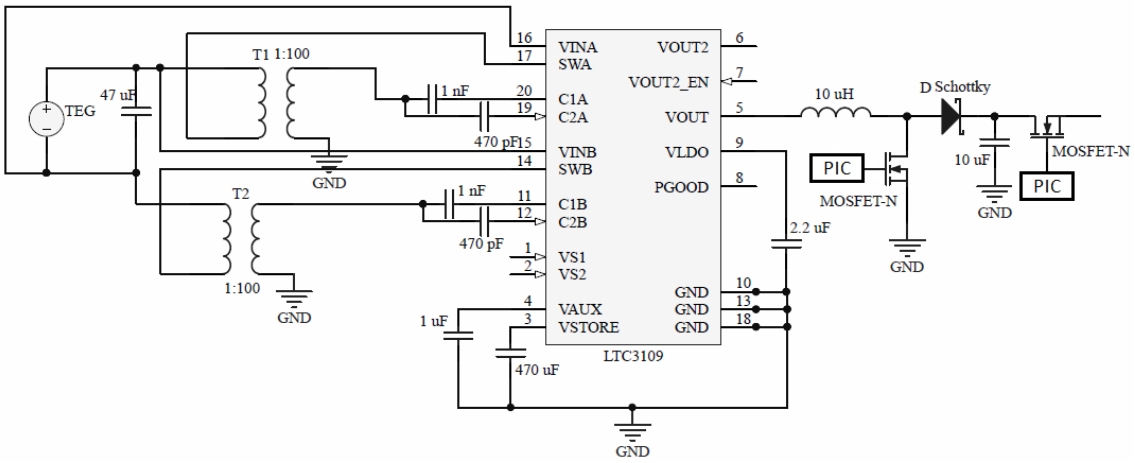

Figure 6.5: Thermoelectric energy harvesting circuit

6.1.4 Battery charger circuit

To charge the battery we use Linear's integrated circuit LTC4071. We chose this part because it is especially designed for energy harvesting applications, or intermittent and low power sources. It also includes some interesting features to prevent battery damage, like a Low Battery Disconnect Function to protect batteries from over-discharge [44]. This chip also permits to select the float voltage, as well as the low-battery threshold voltage to disconnect the battery from the circuit.

When there is an energy source available, the chip powers the load and charges the battery at the same time. If the source disappears or is not enough, the circuit enables the battery to power the load until the battery voltage reaches the low-battery threshold voltage, when the battery is disconnected from the circuit to avoid over-discharge.

When the battery is fully charged and the load requires less power than the given by the source, current is shunted away internally to protect the battery. Although this is not the ideal situation in energy harvesting applications, this case is not very likely to happen, and moreover, the only solution would be to choose a battery with more capacity.

We will use a 3.7 V Li-polymer battery with a capacity of 100 mAh and we configure the circuit so that the float voltage is 4.2 V and the Low Battery Disconnect voltage is 2.7 V. The configuration is shown in Figure 6.6, where the final storage capacitor of the energy harvesting part is also represented. The resistor placed just before the capacitor is used to stand the voltage drop between the capacitors, in case this difference is too high for the corresponding MOSFET, and the diode is used to prevent the capacitor from discharging the battery. The rest of the components have been chosen following the indications in the datasheet [44].

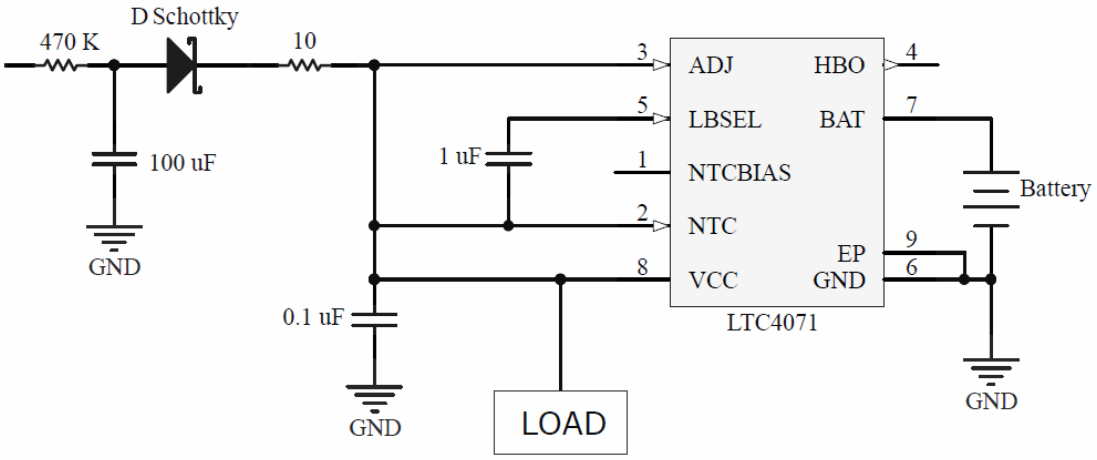

Figure 6.6: Battery charger circuit

6.1.5 Microcontroller

We use the microcontroller incorporated in the Energy Harvesting Development Board, the PIC24F16KA102. For the prototyping phase we decided to use it attached to the Microchip's board, as it includes the required 3.3 V power source, simplifying the connections. As it has been seen before, each energy harvesting part has two N-Channel MOSFETs: the first one (included in the boost topology) regulates the charge of the capacitor, while the second one regulates the power transfer between the first and the second capacitor. The microcontroller is used to measure the voltage of each capacitor and control all the transistors by setting their gate voltage. If the gate voltage is logic high, the MOSFET will be active, while if it is low, it will be open.

The PIC incorporates a high-speed A/D converter that can be configured to measure the voltage at some analog pins. Depending on these values, it will switch on or off the corresponding MOSFET to regulate the power transfer. The maximum voltage permitted in an input pin is around 3.6 V, so we place voltage dividers (not represented in Figure 6.10) to scale the voltage that we need to measure, and then we program the microcontroller so that it shows the real value. Given that the voltage in the capacitor will not be higher than 6 V, we use two identical resistors of 47 kΩ to obtain one half of the voltage, and it is not necessary to place a zener diode in parallel to limit the voltage. Moreover, it was observed that if a 3.3 V zener diode was placed, the output of the voltage divider was not exactly one half of the input voltage, due to the leakage current of the diode.

To explain the algorithm programmed in the microcontroller to control the transistors, we will denominate C_1 the capacitor in a particular energy harvesting part, C_f the final capacitor shared by the three parts, *SW1* the MOSFET that regulates the charge of the first capacitor, and *SW2* the MOSFET that controls the connection between the first and the final capacitor. Figure 6.7 represents the connection between the capacitors in a simplified way, with the nomenclature mentioned before. The logic used to control the transistors can be summarized as follows:

- The microcontroller measures the voltage in C_1 and C_f, which we will denominate V_1 and V_f respectively.

- If V_1 is greater than V_f, *SW2* is enabled to allow the charging of the final capacitor. Moreover, in this case, if V_1 is higher than a certain value that indicates that the capacitor is charged enough, *SW1* will be switched on, while otherwise it will be switched off.
- If V_1 is smaller than V_f, both *SW2* and *SW1* are disabled. As *SW1* is opened, C_1 will charge until the previous case is reached.

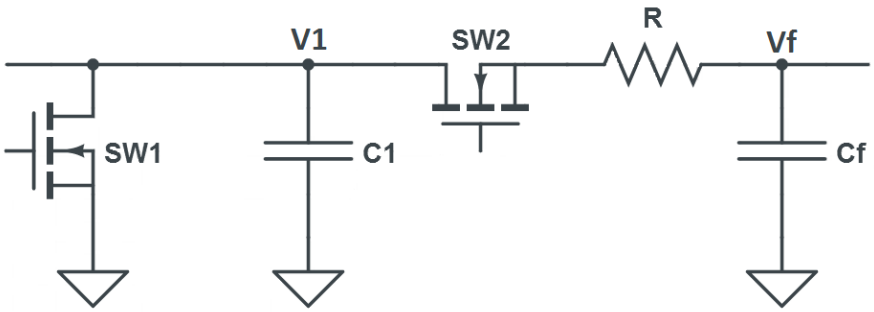

Figure 6.7: Schematic switch circuit

However, when switching on the second MOSFET, it must be taken into account that we cannot connect more than one capacitor to the final capacitor at the same time, as the capacitors corresponding to different sources will be at different voltages. To overcome this problem, the microcontroller measures all the voltages and determines which MOSFETs must be switched on. Then, it commutes the transistors so that they are never closed at the same time. For example, if the microcontroller detects that all the MOSFETs must be switched on, the sequence of commutation will be like in Figure 6.8.

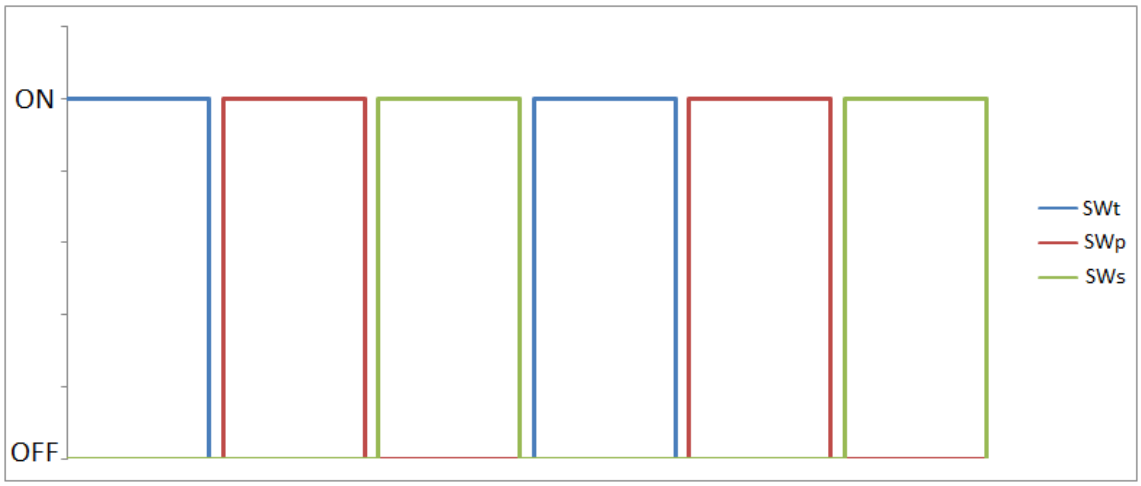

Figure 6.8: Sequence of commutation when all the MOSFETs must be switched on

Moreover, the microcontroller is programmed to measure every second, so the sequence of commutation must last more or less this time. Consequently, the time that a particular MOSFET is ON will depend on how many transistors must be activated during the sequence. That is, if only one of the sources is going to charge the capacitor, the

corresponding MOSFET will be closed almost one second, while if the three sources are going to be connected, each MOSFET will be active around a third of the time.

Figure 6.9 shows the procedure followed by the microcontroller to determine which transistors must be switched on, and Table 6.2 explains the nomeclature used in this diagram.

Table 6.2: Nomenclature used in Figure 6.9

Vs	Voltage of the capacitor in the solar circuit
Vt	Voltage of the capacitor in the thermoelectric circuit
Vp	Voltage of the capacitor in the piezoelectric circuit
Vf	Voltage of the final capacitor
SW1s	MOSFET that regulates the charging of the capacitor in the solar circuit
SW1t	MOSFET that regulates the charging of the capacitor in the thermoelectric circuit
SW1p	MOSFET that regulates the charging of the capacitor in the piezoelectric circuit
SW2s	MOSFET that regulates the connection between the capacitor in the solar circuit and the final capacitor
SW2t	MOSFET that regulates the connection between the capacitor in the thermoelectric circuit and the final capacitor
SW2p	MOSFET that regulates the connection between the capacitor in the piezoelectric circuit and the final capacitor
solarON	If it is 1, SW2s must be switched on
tegON	If it is 1, SW2t must be switched on
piezoON	If it is 1, SW2p must be switched on
Sw	It determines the commutation sequence of the transistors

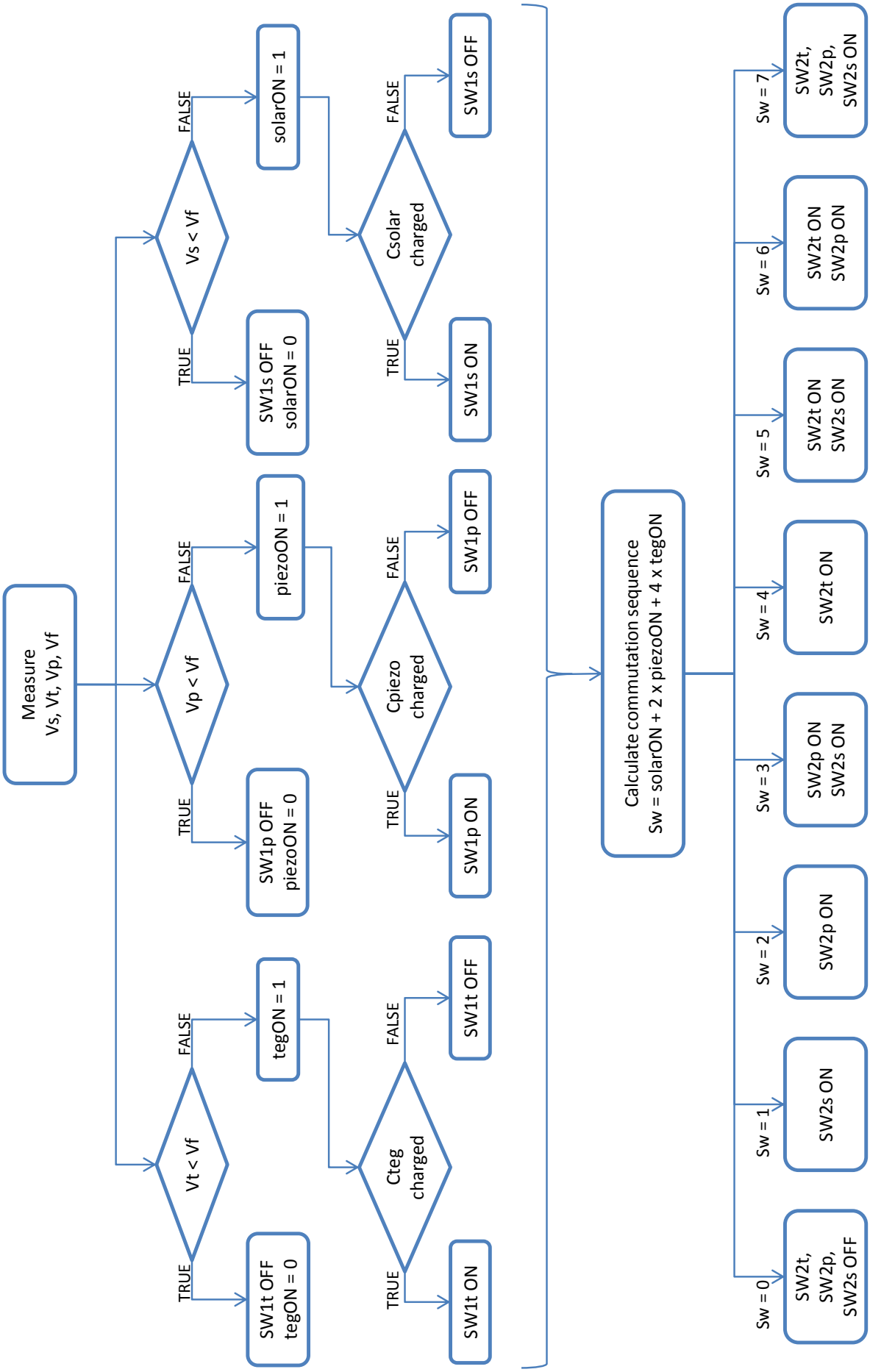

Figure 6.9: Procedure followed by the microcontroller to control the transistors

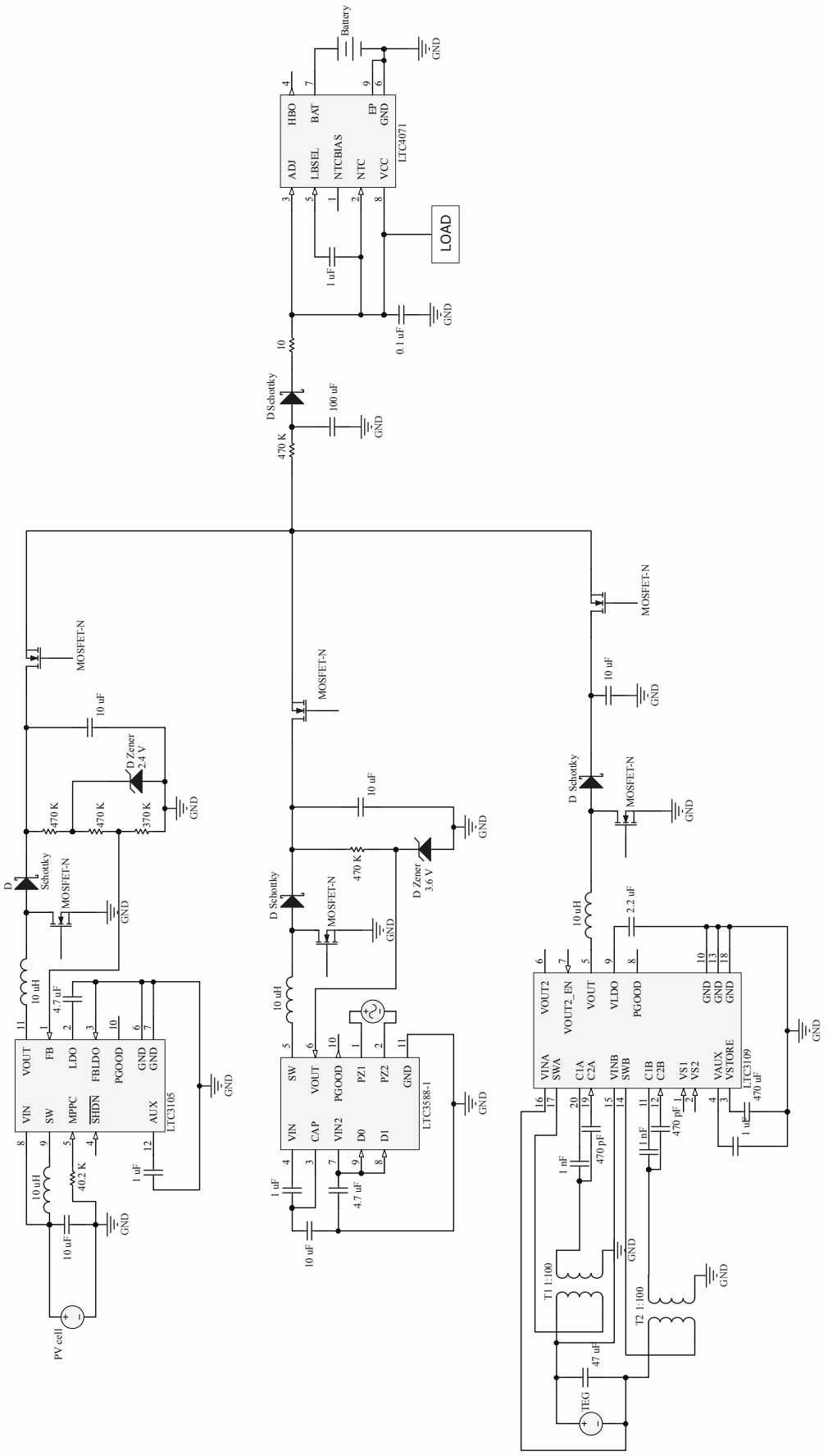

Figure 6.10: Schematic of the whole circuit, excluding the logic circuit and the microcontroller

6.2 Implementation and Results

In the section before we have explained the circuit designed, as well as the role played by the microcontroller. As we have said before, for prototyping we use the XLP 16-bit Energy Harvesting Development Kit, to simplify the connections with the microcontroller and its programming. Table 6.3 indicates the pins used for the connections with the microcontroller, explaining what they are used for, and in Figure 6.11 we can see the pin diagram of the PIC24F16KA102.

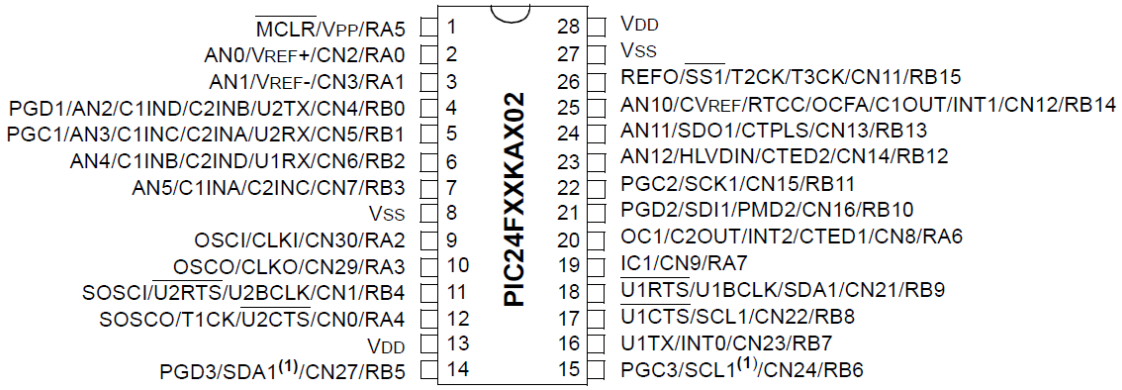

Figure 6.11: PIC24F16KA102 Pin diagram [45]

Table 6.3: Microcontroller pins assignment

Pin Number	Pin Name	Configuration	Task
2	AN0/RA0	Analog Input	Measuring Vt
3	AN1/RA1	Analog Input	Measuring Vp
25	AN10/RB14	Analog Input	Measuring Vs
24	AN11/RB13	Analog Input	Measuring Vf
15	RB6	Digital Output	Controlling SW1t
16	RB7	Digital Output	Controlling SW2t
17	RB8	Digital Output	Controlling SW1p
18	RB9	Digital Output	Controlling SW2p
21	RB10	Digital Output	Controlling SW1s
22	RB11	Digital Output	Controlling SW2s

The rest of the circuit is prototyped on several breadboards, as can be seen in Figure 6.12. For this prototype phase, we use Micropelt thermoelectric generator, the photovoltaic cell used for the parametrization, and Mide V21BL piezoelectric harvester, at a vibration of 40 Hz and a tip mass of 4.8 grams.

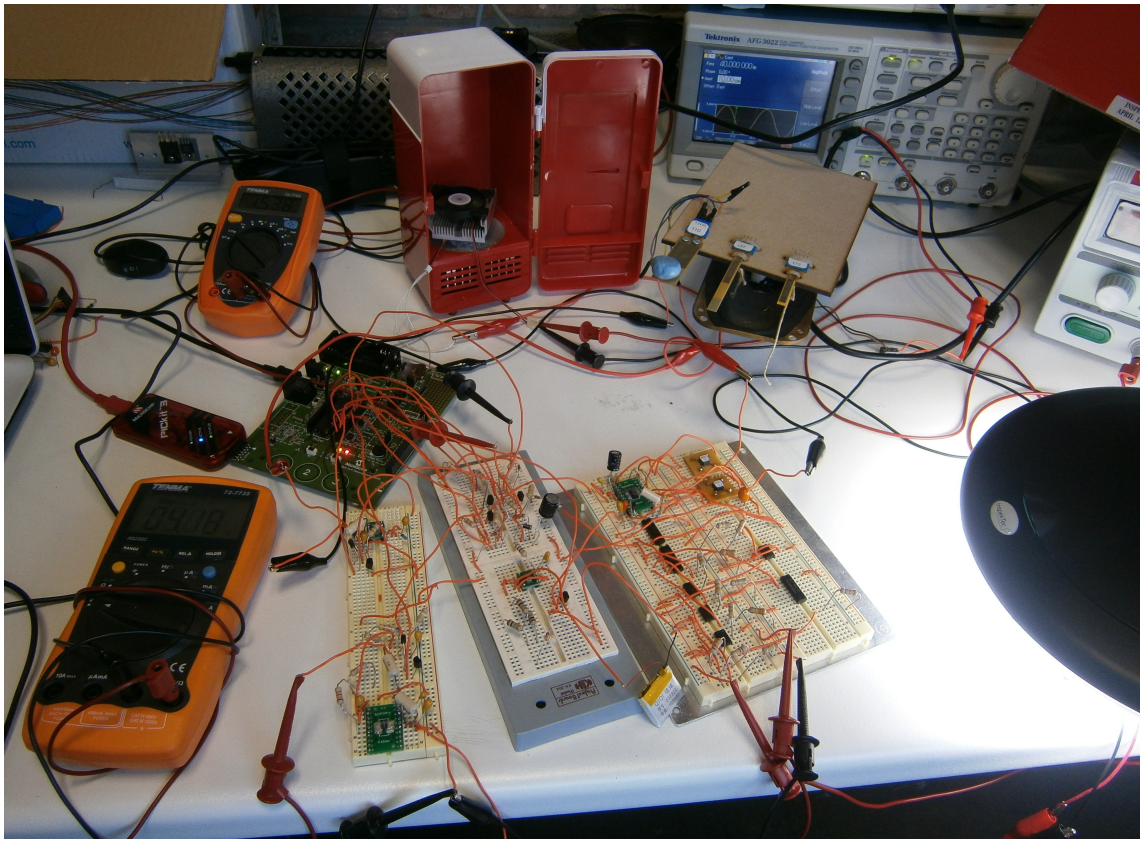

Figure 6.12: Prototype implementation

In Figures 6.13 and 6.14 we can observe the circuits more clearly.

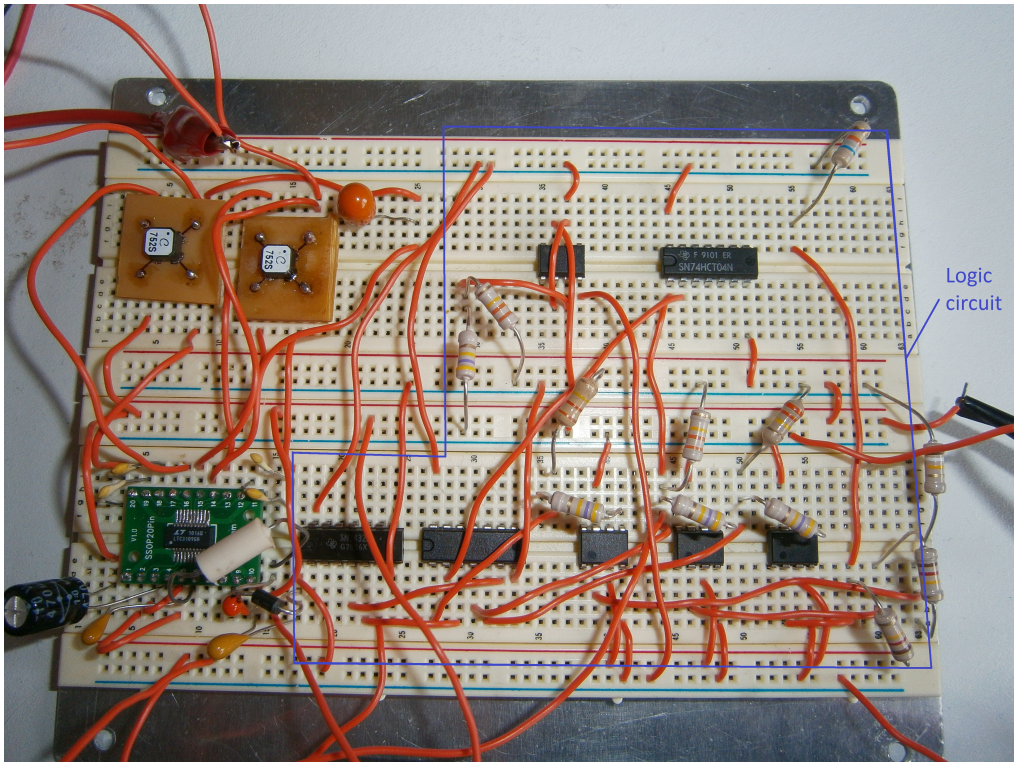

Figure 6.13: Thermoelectric circuit implementation

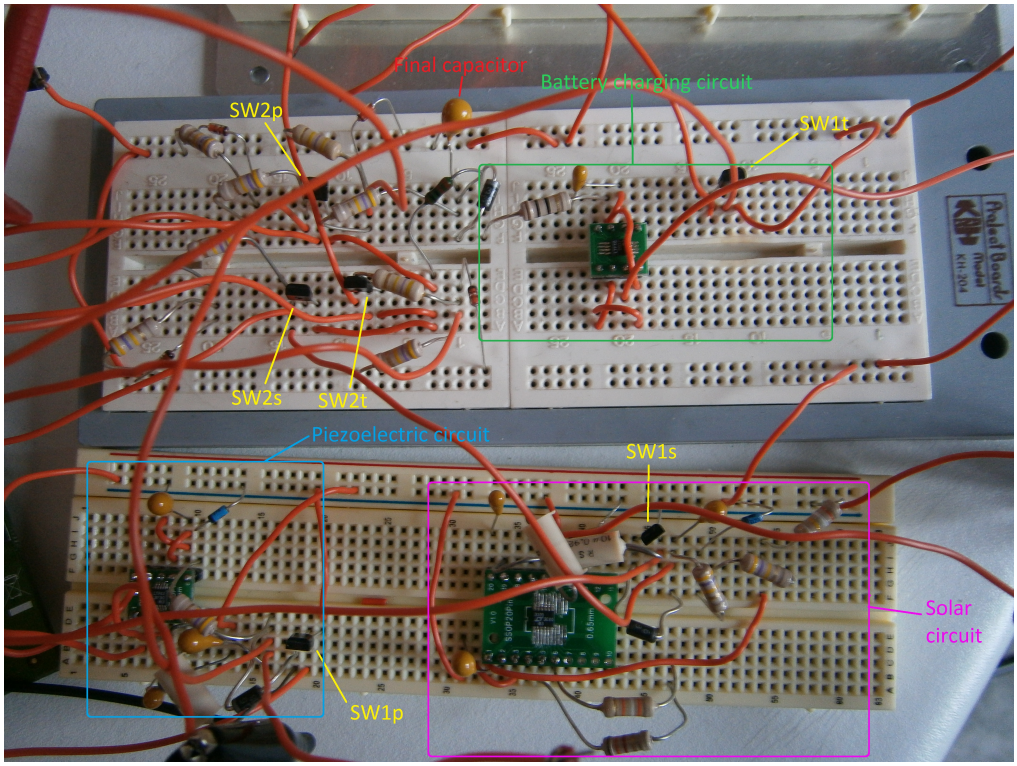

Figure 6.14: Implementation of the rest of the circuit

After making some measurements we realised that the logic circuit used to fix the output of the LTC3109 was well designed but it was not working because it was not powered properly. The logic gates need to be powered with 5 V, so we tried to obtain this voltage from the 12 V power supply (the same as we used for the LM741), using a voltage divider. However, the voltage divider output was much lower than expected (1.8 V), probably because there were too many elements connected to this point. As we did not have other logic gates with a different supply voltage, we decided to fix the output voltage of the LTC3109 to 5 V, although we know it is not the most efficient solution.

Moreover, we tested the circuit using the different sources and we noticed that the voltage of the final capacitor was always 1.6 V at maximum, so the battery charging circuit was never working, because the LTC4071 disconnects the battery when the supply voltage is below the low-battery threshold [44], which we fixed at 2.7 V. The reason why the final voltage could not be higher was that we were trying to control the transistors with a gate voltage of around 3.3 V (the output voltage on any digital pin, according to the datasheet [45]), but as the voltage in the final capacitor increased, the gate-source voltage in the MOSFET decreased, so the transistor was controlling the source voltage (voltage of the capacitor) so that it was equal to the difference between the gate voltage and the Gate Threshold Voltage ($V_{GS(th)}$) (2.1 V according to the datasheet of the transistor [46]). To solve this problem, we replaced the N-channel MOSFETs with two P-channel MOSFETs in series, in a way that their diodes were in opposite directions, as can be observed in Figure 6.15. Although the P-MOSFET has a higher resistance than the N-MOSFET, it is still a good solution given the low value of the currents in this circuit.

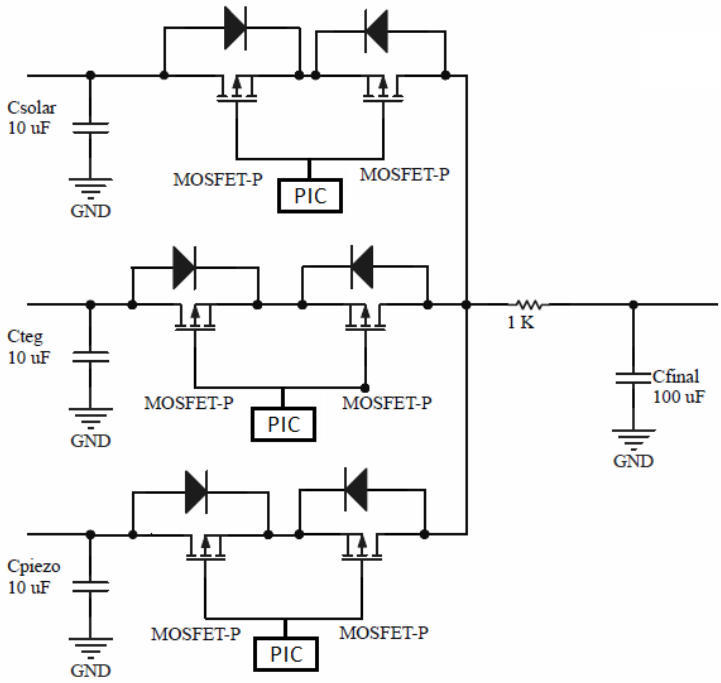

Figure 6.15: Configuration using p-MOSFETS

Obviously, we had to modify the code, as P-MOSFETs are activated with negative V_{GS} voltages. Now, to switch on the MOSFET, we have to set low the corresponding pin. After making this change, the circuit seemed to be working properly, since now the voltage in the final capacitor increased until 3 V. Figure 6.16 shows a screenshot of the terminal

program, with the information sent by the microcontroller. There, we can observe that both the thermoelectric and the solar sources are active, that is, their voltage is higher than the voltage stored in the final capacitor, so their MOSFETs are turned on.

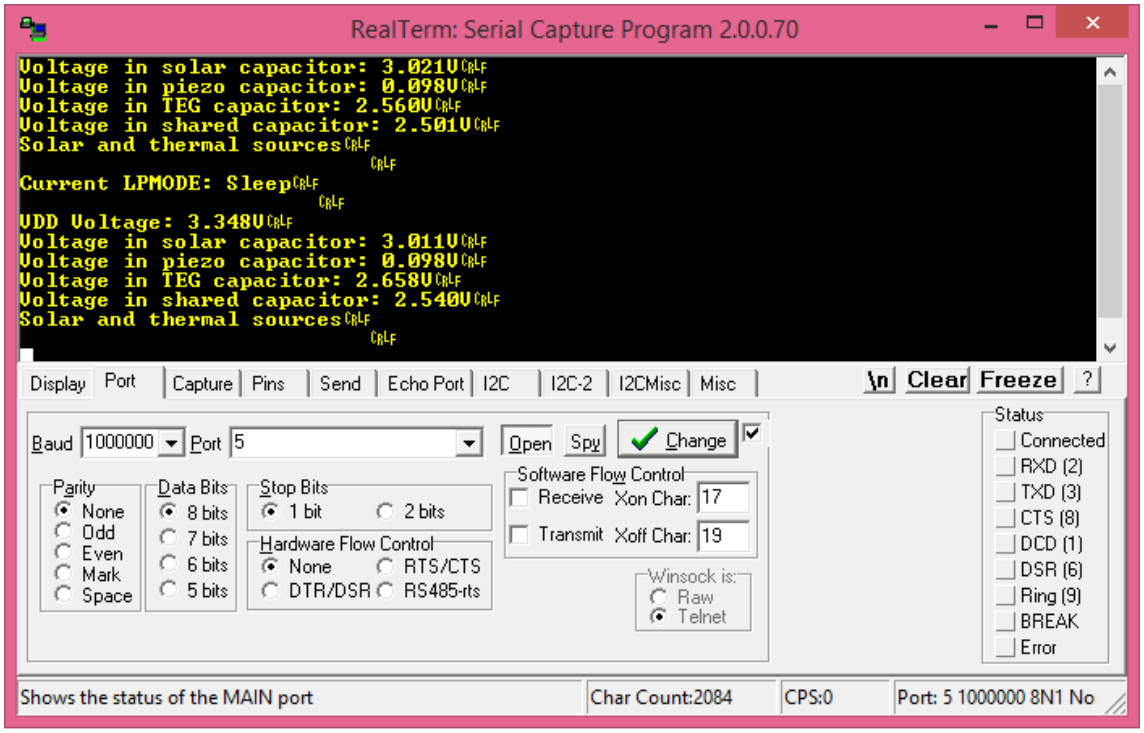

Figure 6.16: Information in the terminal program

However, when we measured the current into the battery charger by measuring the voltage drop accross the resistor placed between the final capacitor and the LTC4071, we found out that all the current was being supplied by the solar source. Indeed, if we disconnected this source, the current was zero. We made more measurements, using one unique source at a time and keeping the corresponding MOSFETs closed all the time, but the results were still the same. If using the solar source, the charging current was around 55 µA, while using the other sources it was zero. In fact, using just the thermoelectric source, the circuit was not even able to charge the final capacitor, and all the voltage stored in the capacitor of the thermoelectric branch was lost in the corresponding MOSFETs.

Finally, we came to the conclusion that this problem was due to a mismatch between the sources and the load. The circuit had been designed supposing that all the sources would behave in a similar way, so it would be possible to switch between them, but apparently, the thermoelectric and the piezoelectric sources are not able to provide current at the same rate that it is drawn from the capacitor. Consequently, when the correponding MOSFETs are switched on, the voltage in the capacitor drops instantaneously, but it never recovers.

Just to test how the battery charger operates, we also tried disconnecting all the sources and connecting a battery as power source. In this case, the charging current was 72 µA, so the solar source actually works pretty well.

To test if the code programmed in the microcontroller works, we replaced the thermoelectric and piezoelectric sources by a battery. Then, we observed that the charging current was varying between 32 µA and 118 µA, while with the battery disconnected it was from 13 to 62 µA. The code actually works as expected, activating the corresponding

MOSFETs when there is a source available. Being the piezolectric circuit off, the voltage in the gates of the solar and thermoelectric MOSFETs (referenced to ground) is shown in Figure 6.17, obtained with the oscilloscope. There, the blue signal corresponds to the solar MOSFET's gate and the yellow one to the thermoelectric (battery) MOSFET's gate, and we can see that the MOSFETs switch alternatively.

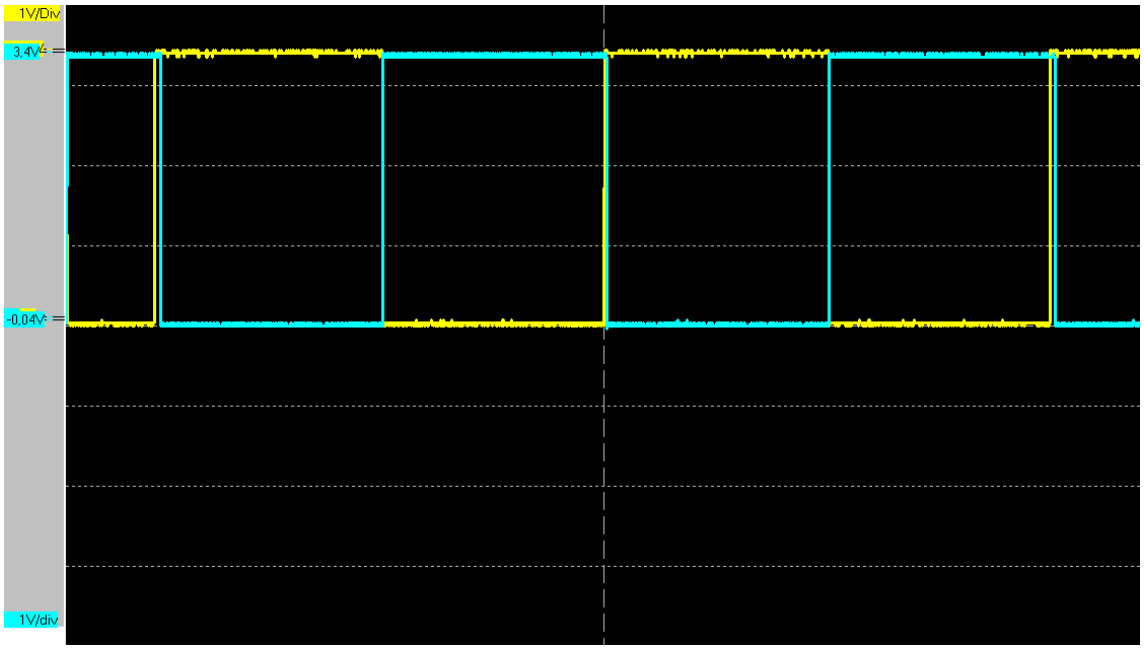

Figure 6.17: Gate Voltage of solar and thermoelectric MOSFETs

Finally, we connected a LED with a resistor in series as a load (Figure 6.18), and we observed that it was blinking intermittently. When the battery was powering the circuit, the current accross the resistor was until 250 µA, and the LED shined much brighter than being powered by the photovoltaic cell.

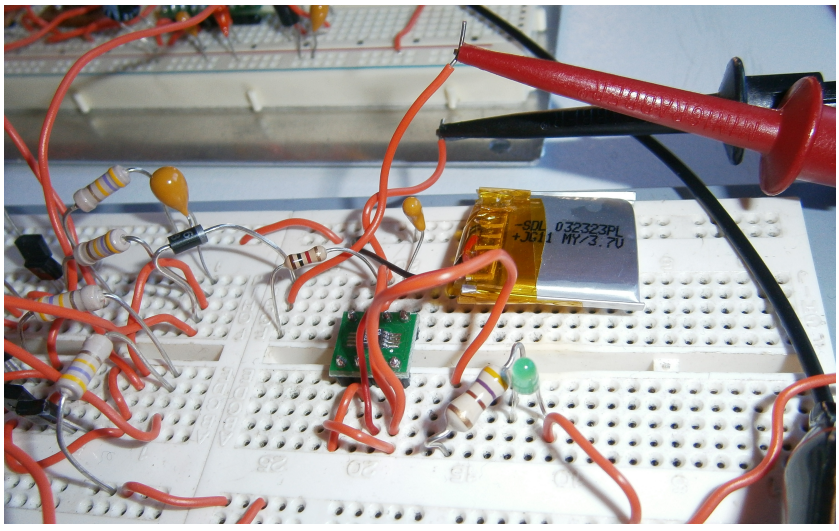

Figure 6.18: LED connected to the LTC4071 as a load

Chapter 7

Conclusions and Future Work

The main purpose of this thesis was to implement a complementary balanced energy harvesting system. We have tested and compared different harvesters commercially available to scavenge energy from three different sources, characterizing their performance in non-ideal conditions.

The system designed is a good approach to the posed problem, but its effectiveness is restricted by the limited efficiency of the harvesters and, above all, by the mismatch between the load and the sources, which makes that only one of the sources is actually employed.

This difficulty could be faced with a switching regulator, or controlling the current injected with the MCU, by measuring the voltage drop accross a resistor placed in series with the capacitor, so that the source is able to recharge the capacitor at the same rate. However, it was unfeasible to implement any of these solutions before the deadline of this thesis.

What remains to be done is to adapt the design to the characteristics of each source and harvester in order to eliminate the mismatch mentioned above, and to improve the experimental setups to harvest energy from vibrations and thermal gradients, as any change in their configuration affects dramatically to their efficiency.

Bibliography

[1] Adnan Harb. Energy harvesting: State-of-the-art. *Renewable Energy*, 36(10):2641–2654, 2011.

[2] RJM Vullers, Rob van Schaijk, Inge Doms, Chris Van Hoof, and R Mertens. Micropower energy harvesting. *Solid-State Electronics*, 53(7):684–693, 2009.

[3] Kai Kang. Multi-source energy harvesting for wireless sensor nodes (thesis). 2012.

[4] Yannick Verbelen, An Braeken, and Abdellah Touhafi. Towards a complementary balanced energy harvesting solution for low power embedded systems. *Microsystem Technologies*, pages 1–15, 2014.

[5] Mary Ann Ingram, Lakshmi Thanayankizil, Jin Woo Jung, and Aravind Kailas. Perspectives on energy-harvesting wireless sensor networks. In *Globalization of Mobile and Wireless Communications*, pages 249–274. Springer, 2011.

[6] Ruud JM Vullers, RV Schaijk, Hubregt J Visser, Julien Penders, and Chris Van Hoof. Energy harvesting for autonomous wireless sensor networks. *Solid-State Circuits Magazine, IEEE*, 2(2):29–38, 2010.

[7] Tim Wogan. Implant harvests heartbeat power. *Royal Society of Chemistry*, 22 Jan 2014.

[8] KA Cook-Chennault, N Thambi, and AM Sastry. Powering mems portable devices: a review of non-regenerative and regenerative power supply systems with special emphasis on piezoelectric energy harvesting systems. *Smart Materials and Structures*, 17(4):043001, 2008.

[9] Shad Roundy, Paul K Wright, and Jan Rabaey. A study of low level vibrations as a power source for wireless sensor nodes. *Computer communications*, 26(11):1131–1144, 2003.

[10] Eugenio Cantatore and Martin Ouwerkerk. Energy scavenging and power management in networks of autonomous microsensors. *Microelectronics journal*, 37(12):1584–1590, 2006.

[11] Cian Ó Mathúna, Terence ODonnell, Rafael V Martinez-Catala, James Rohan, and Brendan OFlynn. Energy scavenging for long-term deployable wireless sensor networks. *Talanta*, 75(3):613–623, 2008.

[12] Harry Zervos. Electromagnetic induction in energy harvesting applications. *Energy Harvesting Journal*, 26 Sep 2013.

[13] Renee Meiller. Vibration energy the secret to self powered electronics. *University of Wisconsin-Madison*, 20 Feb 2014.

[14] Paul D Mitcheson, Tim C Green, Eric M Yeatman, and Andrew S Holmes. Architectures for vibration-driven micropower generators. *Microelectromechanical Systems, Journal of*, 13(3):429–440, 2004.

[15] Linear Technology. *LTC3588-1 Piezoelectric Energy Harvesting Power Supply (Datasheet)*, REV A, Sept 2010.

[16] Oxford Photovoltaics. Oxford research team pioneers semi-transparent perovskite solar cells. *http://www.oxfordpv.com/*, 30 Jan 2014.

[17] Olga Malinkiewicz, Aswani Yella, Yong Hui Lee, Guillermo Mínguez Espallargas, Michael Graetzel, Mohammad K. Nazeeruddin, and Henk J. Bolink. Perovskite solar cells employing organic charge-transport layers. *Nature Photonics*, (8), 22 Dec 2013.

[18] Gordon J. Hedley, Alexander J. Ward, Alexander Alekseev, Calvyn T. Howells, Emiliano R. Martins, Luis A. Serrano, Graeme Cooke, Arvydas Ruseckas, and Ifor D. W. Samuel. Determining the optimum morphology in high-performance polymer-fullerene organic photovoltaic cells. *Nature Communications*, 4, 17 December 2013.

[19] Edgar Meza. Solar frontier sets thin-film pv world record with 20.9

[20] Nathan Bourgoine. Harvest energy from a single photovoltaic cell. *LT Journal of Analog Innovation*, 21(1), April 2011.

[21] Pai H Chou and Sehwan Kim. Techniques for maximizing efficiency of solar energy harvesting systems. *Proc ICMU*, 10:26–28, 2010.

[22] Linear Technology. *LTC3105 400mA Step-Up DC/DC Converter with Maximum Power Point Control and 250mV Start-Up (Datasheet)*, REV A, Feb 2011.

[23] Texas Instruments Incorporated. *Ultra Low Power Boost Converter with Battery Management for Energy Harvester Applications*, Sept 2012.

[24] Harry Zervos. Thermoelectric generators: Vehicles, wireless sensors, industrial apps. *Energy Harvesting Journal*, 13 March 2014.

[25] Raghu Das. The rise of thermoelectrics. *Energy Harvesting Journal*, 24 Oct 2013.

[26] Linear Technology. *LTC3109 Auto-Polarity, Ultralow Voltage Step-Up Converter and Power Manager (Datasheet)*, REV B, August 2013.

[27] Davide Carli, Davide Brunelli, Luca Benini, and Massimiliano Ruggeri. An effective multi-source energy harvester for low power applications. In *Design, Automation & Test in Europe Conference & Exhibition (DATE), 2011*, pages 1–6. IEEE, 2011.

[28] Chulsung Park and Pai H Chou. Ambimax: Autonomous energy harvesting platform for multi-supply wireless sensor nodes. In *Sensor and Ad Hoc Communications and Networks, 2006. SECON'06. 2006 3rd Annual IEEE Communications Society on*, volume 1, pages 168–177. IEEE, 2006.

[29] Saurav Bandyopadhyay and Anantha P Chandrakasan. Platform architecture for solar, thermal, and vibration energy combining with mppt and single inductor. *Solid-State Circuits, IEEE Journal of*, 47(9):2199–2215, 2012.

[30] Microchip Technology Inc. *XLP 16-bit Energy Harvesting Development Kit*, August 2011.

[31] Texas Instruments. *eZ430-RF2500-SEH Solar energy harvesting development kit - Product Bulletin*, 2009.

[32] Cymbet Corporation. *CBC-EVAL-08, EnerChip^{TM} EH Solar Energy Harvester Evaluation Kit*, Rev18, 2009.

[33] Arveni. *T. REX Vibration Energy Harvester Datasheet*, Version 1, Jan 2013.

[34] Mide. *Mide Volture Piezoelectric Energy Harvesters Data Sheet*, Rev. 002, 01-23-2013.

[35] Nextreme Thermal Solutions. *eTEG HV37 Power Generator Data Sheet*, Rev. 1.0.

[36] Micropelt. *TGP-751, TGP-651 ThermoGenerator - Package(TGP). Thin Film Thermogenerator inside standard package. Preliminary Datasheet.*, Version 2.3, Feb 2013.

[37] Marlow Industries Inc. *EHA-PA1AN1-R02-L1 Thermal Energy Harvesting Demo Unit Solid to Air. TECHNICAL DATA SHEET Preliminary*, REV 3.

[38] Microchip Technology Inc. *XLP 16-Bit Development Kit Users Guide*, Rev. B, June 2010.

[39] Davy Van Belle. Unpublished master thesis: Ontwikkeling van een modulaire testopstelling voor onderzoek van laag vermogen indoor fotovoltasche cellen (development of a modular test-bed for research on low power indoor photovoltaic cells). 2014.

[40] Phywe. *Operating instructions 06752.05, 06752.04, 06752.03 (Datasheet).*

[41] E Siivola, R Mahadevan, P Crocco, K Von Gunten, and D Koester. Design considerations for teg system optimization. *Nextreme Thermal Solutions, Inc. Whitepaper*, 2010.

[42] Aldo Romani, Rudi Paolo Paganelli, Enrico Sangiorgi, and Marco Tartagni. Joint modeling of piezoelectric transducers and power conversion circuits for energy harvesting applications. *Sensors Journal, IEEE*, 13(3):916–925, 2013.

[43] Microchip Technology Inc. *MCP601/1R/2/3/4 2.7V to 6.0V Single Supply CMOS Op Amps (Datasheet)*, Rev. G, Dec 2007.

[44] Linear Technology. *LTC4071 Li-Ion/Polymer Shunt Battery Charger System with Low Battery Disconnect (Datasheet)*, REV C, Nov 2011.

[45] Microchip Technology Inc. *PIC24F16KA102 Family Data Sheet. 20/28-Pin General Purpose, 16-Bit Flash Microcontrollers with nanoWatt XLP Technology*, Rev. C, October 2011.

[46] Fairchild Semiconductor. *2N7000 / 2N7002 / NDS7002A N-Channel Enhancement Mode Field Effect Transistor*, Rev. A1, November 1995.